Article:
Bar, L, Dejeu, J, Lartia, R et al. (4 more authors) (2020) Impact of antigen density on recognition by monoclonal antibodies. Analytical Chemistry. ISSN 0003-2700

https://doi.org/10.1021/acs.analchem.0c00092

Impact of antigen density on recognition by monoclonal antibodies

Laure Bar,[†] Jérôme Dejeu,[†] Rémy Lartia,[†] Fouzia Bano,[‡] Ralf P. Richter,[‡] Liliane Coche-Guérente*[,†] and Didier Boturyn*[,†]

[†]Univ. Grenoble-Alpes, CNRS, DCM UMR 5250, 570 rue de la chimie, CS 40700, 38058 Grenoble Cedex 9, France.

Email: didier.boturyn@univ-grenoble-alpes.fr

[‡]University of Leeds, School of Biomedical Sciences, Faculty of Biological Sciences, School of Physics and Astronomy, Faculty of Engineering and Physical Sciences, Astbury Center for Structural Molecular Biology, and Bragg Centre for Materials Research, Leeds, United Kingdom

ABSTRACT: Understanding antigen-antibody interactions is important to many emerging medical and bioanalytical applications. In particular, the levels of antigen expression at the cell surface may determine antibody-mediated cell death. This parameter has a clear effect on outcome in patients undergoing immunotherapy. In this context, CD20 which is expressed in the membrane of B cells has received significant attention as target for immunotherapy of leukemia and lymphoma using the monoclonal antibody rituximab. To systematically study the impact of CD20 density on antibody recognition, we designed self-assembled monolayers that display tunable CD20 epitope densities. For this purpose, we developed in situ click chemistry to functionalize SPR sensor chips. We find that the rituximab binding affinity depends sensitively and non-monotonously on CD20 surface density. Strongest binding, with an equilibrium dissociation constant (K_D = 32 nM) close to values previously reported from in vitro analysis with B cells (apparent K_D between 5 and 19 nM), was obtained for an average inter-antigen spacing of 2 nm. This distance is required for improving rituximab recognition, and in agreement with the known requirement of CD20 to form clusters to elicit a biological response. More generally, this study offers an interesting outlook in the understanding of the necessity of epitope clusters for effective mAb recognition.

Despite the continuous improvement of traditional chemotherapy, the use of monoclonal antibodies (mAbs) as drugs for the treatment of a variety of diseases has been growing steadily for the last two decades.[1] In this context, there is a strong interest in studying mAb recognition of cognate antigens. MAbs are used in oncology for many therapeutic targets including the CD20 antigen, the human epidermal growth factor receptor 2 (HER2), the vascular endothelial growth factor (VEGF), the epidermal growth factor receptor (EGFR) and the programmed cell death protein 1 (PD-1).[2] The hematopoietic differentiation antigens associated with cluster of differentiation (CD) represent the main targets for mAb in oncology.[3] In particular, the CD20 antigen is the target of several therapeutic mAbs and their derivatives (e.g. rituximab, ibritumomab, ofatumumab, obinutuzumab, ocrelizumab) that are successfully used to treat B-cell malignancies, including non-Hodgkin's lymphoma and chronic lymphocytic leukemia, as well as some autoimmune disorders such as rheumatoid arthritis, systemic lupus erythematosus and multiple sclerosis.[4]

The antigen-binding activity of mAbs determines their biological efficacy and depends on several factors, including antigen density, association and dissociation rates. Several studies have suggested that the increase of CD20 antigen expression modulates the biological response of mAbs such as complement-dependent cytotoxicity (CDC) and antibody-dependent cellular cytotoxicity (ADCC) that trigger cell death.[5,6,7] As the antigen distribution generally has a direct impact on the clinical efficacies of mAbs, it is of interest to study the influence of CD20 density on mAb recognition. CD20-rituximab (RTX) interactions have been studied in vitro on B-cell lymphoma lines by using flow cytometry or gamma counter experiments.[8,9] Equilibrium dissociation constants (K_D) in the nanomolar range (5-19 nM) have been reported. These studies, however, did not assess the antigen surface density and distribution. Consequently, it remains unknown how RTX binding to CD20 depends on CD20 surface density, and if the measured dissociation constants are representative of high or low CD20 densities. To date, such information is rarely available for any mAb/antigen combination of clinical relevance highlighting the need for new methods to characterize how mAb recognition depends on antigen density.

Label-free solid-phase interaction assays with highly defined biofunctional surfaces can overcome the limitations of cell-based assays, and enable quantitate antigen-antibody interaction analysis. Initial kinetic studies concerning CD20-RTX interactions performed by SPR analysis have shown important variation of the equilibrium dissociation constants (K_D) values, spanning from a few hundred nanomolar to several micromolar.[10,11] The disparity in K_D values reported for solid-phase versus cell-based binding assays could be related to differences in the accessibility of the immobilized CD20 epitope. In particular, commercial SPR sensors rely on the engrafting of the antigen within a three-dimensional (albeit thin) hydrogel matrix which may impose steric constraints to mAb binding. CD20 as a trans-membrane protein is well-oriented on the cell surface, and one can expect to improve recognition if this two-dimensional antigen presentation was reproduced in SPR assays.

A number of strategies have been reported to immobilize peptide probes onto gold surfaces (as required for SPR) for designing peptide-microarrays [12] or peptide-based biosensors.[13] These involve the direct adsorption of thiolated peptides (by the way of cysteine) [14,15] or a covalent coupling of the peptide to preformed self-assembled monolayers (SAMs) of alkanethiols previously adsorbed on the gold substrate. For the latter purpose, Cu(I)-catalyzed azide-alkyne cycloaddition (CuAAC) has been demonstrated to be well suited for the chemical grafting of peptides onto surfaces via an azide-displaying SAM.[16-19] This chemoselective ligation is generally characterized by quantitative yields and fast reaction kinetics. In addition, the triazole moiety generated by the reaction between azide and alkyne was shown to be remarkably inert resulting in a chemically highly stable peptide-functionalized surface.

In the present work, we have examined the dependence of the binding affinity of RTX on CD20 epitope surface density, which is known to be a critical point for the therapeutic response. To this end, the characterization of the peptide functionalized-surface and the binding assays were achieved by using surface sensitive techniques such as quartz crystal microbalance (QCM-D) and surface plasmon resonance (SPR). These label-free detection techniques provide quantitative information on the amount of CD20 peptide grafted on the SAM gold substrate, and also kinetic and thermodynamic parameters of the binding events between CD20-functionalized surfaces and RTX.

EXPERIMENTAL SECTION

All organic compounds were purchased from VWR International S.A.S. (Fontenay-sous-Bois, France), Sigma-Aldrich (Saint-Quentin Fallavier, France), unless otherwise specified in the text. Rituximab (MabThera) was provided gracefully by Genentech, Inc. (San Francisco, US). Solution of infusion was provided at a concentration of 10 mg/mL (i.e. 69.5 µM).

Synthesis of CD20 epitope and CD20 scramble. The CD20 peptide used in this study corresponds to a 25-amino-acid sequence that is located in the extracellular part of the full CD20 protein. The CD20 scramble peptide used as a reference was composed of the same amino-acids in a distinct order. The CD20 and CD20 scramble sequences are NIYNCEPANPSEKNSPSTQYCYSIQ and SATNCNSEYQNEPNYIPYSQCKPIS respectively. Whilst both sequences possess a C5-C21 disulfide bridge, all other peptides were in a randomly selected order for the CD20 scramble. Synthesis of the protected peptides was carried out using the Fmoc/*t*-Bu strategy on a peptide synthesizer (Syro2, Biotage) using 2-chlorotritylchloride®. Reaction with 4-pentynoic acid was performed on the resin to incorporate the alkyne function at the N-terminus. After cleavage and removal of protecting groups, formation of disulfide bridges was performed under oxidative conditions. Peptides were then purified by RP-HPLC and their concentration quantified by a UV spectrophotometer (See the supporting information).

QCM-D measurements. Measurements were performed with a Q-Sense E4 system equipped with 4 independent flow modules (Biolin Scientific, Västra Frölunda, Sweden). The system was operated in flow mode with a flow rate of typically 10 µL/min using a peristaltic pump (ISM935C, Ismatec, Zurich, Switzerland). The working temperature was 25°C. Frequency shifts Δf and dissipation shifts ΔD were measured at six overtones (n = 3, 5, 7, 9, 11, 13), corresponding to resonance frequencies of $f_n \approx 5, 15, 25, 35, 45, 55, 65$ MHz; changes in dissipation and normalized frequency, $\Delta f = \Delta f_n/n$, of the seventh overtone (n = 7) are presented. Any other overtone would have provided comparable information.

Surface preparation. Prior to each QCM-D measurement, QCM-D sensors were cleaned by rinsing with ultrapure water, blow-drying with N_2 and exposure to UV/ozone (Jelight, Irvine, CA, USA) for 10 min. Within 5 min after UV/ozone treatment, the sensors were immersed in an ethanolic solution of HS-$(CH_2)_{11}$-$(EG)_6$-N_3 and HS-$(CH_2)_{11}$-$(EG)_6$-OH (ProChimia Surface, Poland), at a total concentration of 1 mM and the desired molar ratio of thiol-azide to thiol-hydroxyle. After overnight incubation, the sensor surfaces were rinsed with ethanol and blow-dried with N_2 gas, before being installed in the QCM-D modules.

Monitoring of the covalent peptide grafting and binding assays using QCM-D. For the covalent peptide grafting, ultrapure water was first injected in the measurement chamber until reaching a stable baseline. DMSO:H_2O (1:1) as running solution was then injected at a standard flow rate of 10 µL/min. Degassed solutions were injected in the measurement chambers, including CD20 alkyne/CD20-scramble alkyne (200 µM), $CuSO_4$ (500 µM), Tris[(1-benzyl-1H-1,2,3-triazol-4-yl)methyl]amine (TBTA) (500 µM), and (+)-sodium L-ascorbate (3 mM). After reaching the plateau, the sensor surfaces were rinsed with DMSO:H_2O (1:1). For the binding assay, functionalized surfaces were incubated in PBS (1×), citrate (3 mM) and P80 (0.005%) running buffer. Rituximab was then injected in QCM-D module at various concentrations in PBS. The sensor surfaces were rinsed after reaching the plateau. For binding assays carried out for determining the K_D, 30 s injections of Glycine-HCl (10 mM, pH 2) were performed between each RTX concentration.

SPR analysis. SPR data were obtained on a Biacore T200 (GE Healthcare). Measurements were performed on gold surfaces. Sensor chips were cleaned by UV-ozone treatment during 10 min after being rinsed with ultrapure water and ethanol. The cleaned gold surfaces were then functionalized according to the following procedure. Firstly, mixed self-assembled monolayers (SAMs) were formed at room temperature by immersing gold-coated sensors overnight in a thiol mixture of varying percentages of HS-$(CH_2)_{11}$-EG_6-N_3 and HS-$(CH_2)_{11}$-EG_4-OH (1 mM total thiol concentration in EtOH). Sensor chips were rinsed with ethanol and blow-dried with nitrogen gas. The surfaces were then inserted in the Biacore T200 device. For the grafting of CD20 antigen, manual runs were conducted with water as running solvent at 2 µL/min.

The azide-alkyne cycloaddition permitted the covalent grafting of CD20 scramble on channel 1 for the reference, and CD20 on channel 2. Degassed solutions injected are composed of CD20 alkyne/CD20-scramble alkyne (200 µM), $CuSO_4$ (500 µM), Tris[(1-benzyl-1H-1,2,3-triazol-4-yl)methyl]amine (TBTA) (500 µM), and (+)-sodium L-ascorbate (3 mM), in DMSO:H_2O (1:1). Because the microfluidic system is sensitive to high concentrations of DMSO, the time of injection was controlled and optimized at 8 min for each channel, with a 8 min wait between each injection. The large change of solution refractive index during the injection prevents monitoring of the grafting process in real-time. However, the quantity of immobilized antigen could be evaluated by comparing the

shifts in resonance units before and after the injection (Fig. S1 in the supporting information).

The SPR-Biacore experimental conditions were optimized concerning on the one hand the tethering of CD20 (especially the incubation time of CuAAC reactants dissolved in H_2O:DMSO mixture) and on the other hand the composition of the buffer for RTX binding assays (Fig. S3 in the supporting information). The optimized running buffer (RB) consisted of PBS (1×), citrate (3 mM) and polysorbate P80 (0.005%). Flow cell 1 was functionalized with CD20 scramble to provide a reference surface. Binding assays were conducted using a flow rate of 30 µL/min at 25°C. The stability of the CD20-functionalized surface was also been checked by achieving tests of repeatability of RTX binding on CD20-functionalized flow-cells (Fig. S5 in the supporting information). RTX dissolved in RB was injected at different concentrations using the high performance method (injection time: 4 min, stabilization time: 10 min). The RTX concentrations investigated are the following: 5, 10, 20, 50, 100, 200, 500, 1000 nM. A regeneration step was necessary between each RTX injection, and was performed by injecting a solution of Glycine-HCl (10 mM, pH 2) for 10 s. Prior to curve fitting analysis, the binding sensorgrams were double-referenced using reference flow cell 1 and preceding buffer blank subtractions to remove the non-specific adsorption of RTX and the change in refractive index respectively. The binding rate constants of CD20/RTX interactions were calculated by a nonlinear analysis of the association and dissociation phases using the SPR kinetic evaluation software of Biacore T200 (evaluation Software 2.0.1). The data were fitted using a heterogeneous ligand model, which provides the best fitting (Fig. S6 in the supporting information). The reported values are the average of representative independent experiments and the errors provided are standard deviations from the mean. Each SPR experiment was repeated at least four times.

Fab generation. RTX Fab fragments were generated from papain digestion of the mAb by using the Pierce Fab preparation kit (Thermo Scientific) and following the given instructions. Fab fragments were then purified with column provided by the kit. The digestion was checked by SDS-PAGE (Fig. S8 in the supporting information), and Fab fragments concentration was measured by UV.

RESULTS AND DISCUSSION

Control and characterization of CD20 density on gold substrates. We used the extracellular loop of the CD20 protein (amino acids N163 to Q187) which is known to be the binding epitope of RTX.[20] This peptide was prepared by classical solid-phase peptide synthesis and a disulfide bridge formation in buffered solution (see the supporting information). We introduced an alkyne function at the N-terminus for CuAAC coupling to preformed SAM surfaces displaying azide groups (Fig. 1), as previously described.[21,22] Thanks to this site-specific ligation, and the disulfide bridge present in the natural peptide sequence, the CD20 epitope is displayed with a defined orientation and conformation that recapitulates the presentation of the extracellular CD20 loop on the cell surface.[20] The SAM contained alkanethiolates with terminal-oligo(ethyleneglycol) (OEG) that provides physical rigidity in combination with chemical flexibility. Moreover, the OEG-alkanethiols form a bioinert background conferring resistance to non-specific protein adsorption.[23] The SAMs presenting azide were adsorbed on gold substrates by incubating thiol solutions with varying molar ratios of HS-$(CH_2)_{11}$-$(EG)_6$-N_3 (thiol-azide) and HS-$(CH_2)_{11}$-$(EG)_4$-OH (thiol-hydroxyle). By using thiol-azide fractions ranging from 0.1% to 50%, we were able to design functional surfaces with tunable coverages of the CD20 epitope (Fig. 1, Fig S2 in the supporting information).

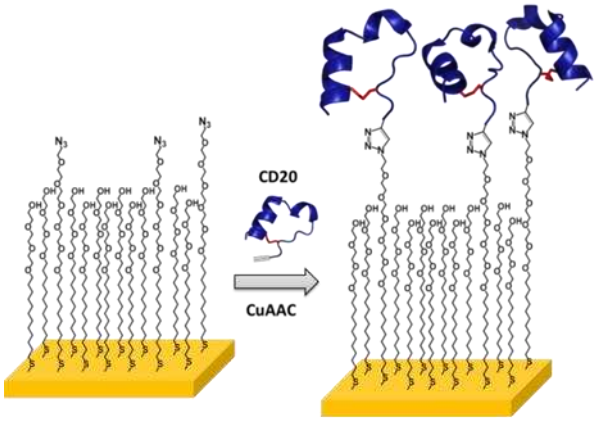

Figure 1. Schematic representation of the CD20 epitopes grafting onto a preformed SAM-azide by CuAAC. The disulfide bridge is shown in red.

In order to control the CD20 surface coverage, two mass-sensitive surface techniques, QCM-D and SPR, were employed. While no measurable change in QCM-D signals (i.e. shifts in frequency, *f*, and dissipation, *D*) was recorded during the injection of CD20 solution without the CuAAC reactants in the flow chamber, a fast decrease in frequency was observed when the reaction mixture containing the CD20 epitope was injected, indicating covalent grafting of CD20 to the SAM-gold substrate (Fig. S9-S10 in the supporting information). Rinsing with pure solvent led to stable signals showing the stability of CD20-functionalized surfaces, and thus providing further evidence of the chemical grafting of the peptide to the surface. The QCM-D traces showed only small shifts in dissipation after CD20-functionalization, indicating that the CD20 epitope form a relatively rigid film. The Sauerbrey relation (Eq. S2) can thus be applied for the determination of the acoustic mass (m_{QCM}; Table 1). QCM-D provides hydrated masses (mass of CD20 layer with hydrodynamically coupled water) which show increasing values until reaching a maximum at 432 ng/cm^2 for 12.5% of thiol-azide.

Following the procedure as established by QCM-D, the covalent grafting of CD20 was transferred to SPR sensors. Grafting was carried out inside the Biacore apparatus onto SAM-functionalized sensor chips, as this enabled different measurement channels to be functionalized with various peptides. In particular, a scramble containing the same amino acids as the CD20 peptide but in a different random order was chosen as reference to be able to correct for variations in the solution refractive index and/or spurious non-specific interactions.

To the best of our knowledge, there are very few examples of *in situ* grafting of SPR sensor chips through CuAAC using an SPR apparatus equipped with a microfluidic system.[24] To prevent damage to the microfluidic system, the hydro-organic solution (H_2O/DMSO) containing the click chemistry reactants was injected only for a short time (8 min) in the flow cells (Fig. S1 in the supporting information). An additional benefit of the *in situ* click chemistry is that it allows quantitating the

amount of grafted CD20 from the change in the SPR signal. By using Jung's formula (Eq. S1 in the supporting information) the magnitude of the response units (RU) was converted into areal mass densities. Jung's formula requires the SAM and CD20 to be considered as separate layers, and the layer thicknesses to be known. These were measured by spectroscopic ellipsometry (SE) (See the supporting information). Whatever the azide percentage, the thickness of the SAM was found to be of 2.5 ± 0.5 nm, in accordance with previous results (2.6 nm).[25] After CD20 grafting at saturation, an additional film thickness of 4.6 ± 0.2 nm was found. The areal mass densities of CD20 calculated from SPR experiments show that the immobilization capacity of the SAM-azide substrate increases monotonously with the number of azide reactive functions across the probed range from 0 to 50% of thiol-azide (Table 1). A comparison of the areal mass densities measured by QCM-D (m_{QCM}; hydrated mass) and by SPR (m_{SPR}; dry mass) provides a measure of the CD20 film hydration (Eq. S3 in the supporting information): the hydration is high (92%) for low CD20 density (2.8 pmol.cm^{-2} corresponding to m_{SPR} of 8 ng.cm^{-2}) and decreases for denser CD20 layers, down to 38% at 85 pmol.cm^{-2} (m_{SPR} = 249 ng.cm^{-2}). The decrease of coupled water induced by lowering the surface coverage as sensed by QCM-D has ever been reported and modeled for globular proteins.[26] The authors showed that the hydration curves could be well fitted by a straight line by using a model that ascribed a hydration coat (truncated pyramid-shaped) to each adsorbed biomolecule. Furthermore, we noticed that to reach a CD20 surface density of 46 pmol.cm^{-2} (m_{SPR} = 135 ng.cm^{-2}) only 6% of azide-presenting alkanethiols would be required in the SAM (since total alkanethiol surface density is 7.3 10-10 mol.cm^{-2}).[22] The mismatch with the 12.5% thiol-azide used in the solution to prepare the SAMs is likely due in part to preferential binding of the thiol-hydroxyl, as previously reported.[22] Additionally, for high thiol-azide densities, the CuAAC reaction may be incomplete due to steric hindrance of CD20 on surface.

Assuming a random distribution of CD20 epitopes on the SAM surface, root-mean-square (rms) distances between adjacent CD20 epitopes were calculated based on the SPR data. Values ranging from 9.1 to 1.4 nm were obtained for surfaces prepared with thiol-azide fractions ranging from 0.1% to 50%, respectively (Table 2).

Table 1. Influence of thiol-azide molar ratio on CD20 areal mass densities.

N_3 (%)	$-\Delta f_7$ (Hz)	m_{QCM}[a] (ng.cm^{-2})	SPR resp.[b] (RU)	m_{SPR}[c] (ng.cm^{-2})	Hydration (%)
0.1	nd	nd	60 ± 11	6 ± 1	nd
1	5.6 ± 0.2	100 ± 4	82 ± 22	8 ± 2	92 ± 2
2.5	14 ± 2.0	251 ± 3	694 ± 118	69 ± 12	72 ± 1
12.5	24 ± 1.0	432 ± 9	1352 ± 308	135 ± 31	69 ± 7
20	23.4 ± 1.3	421 ± 23	1642 ± 381	164 ± 38	61 ± 7
50	22.4 ± 0.6	404 ± 11	2488 ± 145	249 ± 14	38 ± 2

nd = not determinated. (a) Acoustic mass determined with Sauerbrey equation and 7th overtone. (b) SPR Response corresponding to the change of baseline magnitude before and after grafting. (c) Optical mass calculated following Jung's formula (Eq. S1 in the supporting information).

Effect of CD20 density on rituximab recognition. The specificity of the resulting CD20 functionalized surface towards RTX binding affinity was again evaluated by QCM-D and SPR. Using QCM-D, a comparison of two functionalized-surfaces displaying the CD20 epitope and the CD20 scramble respectively clearly demonstrated successful and fully selective binding of RTX (10 nM) to CD20 (Fig. S9 in the supporting information). Additional SPR experiments were carried out to confirm the specificity of the recognition event. Injection of RTX (at 1 µM) to a surface presenting the CD20 epitope led to a response of 1800 RU, whereas only 100 RU were measured with the CD20 scramble and 60 RU with a pure and inert alkanethiolate SAM (Fig. 2). We attribute the 60 RU shift to refractive index effects (which are known to sensitively affect the SPR response), and the difference of 40 RU to non-specific binding. Thus, non-specific binding was very low, justifying the use of the CD20 scramble as the reference channel in all subsequent analyses. Moreover, the complete absence of a response (after subtraction of the reference channel) for an equal concentration of trastuzumab, a mAb which belongs to the same IgG subclass, demonstrates the specificity of the CD20 surface for RTX (Fig. 2, orange curve, Fig. S4, Fig. S12 in the supporting information).

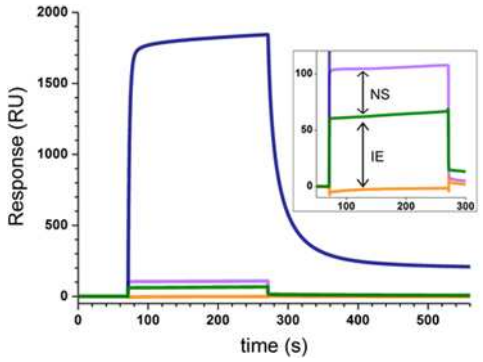

Figure 2. SPR sensorgrams representing control experiments. Raw curves are shown for RTX injections at 1 µM onto SAMs with CD20 epitope (blue), with a CD20 scramble (purple), and without any peptide functionalization (pure thiol-hydroxyle; green). Inset: Zoom into a part of the data. The response on the peptide-free surface is caused by refractive index differences between the pure and mAb containing solutions, whereas the small additional response on the CD20 scramble likely reflects minor and transient non-specific (NS) mAb binding. The specificity of CD20 antigen for RTX is evaluated by the injection of trastuzumab (1 µM) onto the CD20 flow cell (orange curve obtained after subtraction of CD20 scramble reference data). The CD20 and CD20 scramble surfaces were made from functionalized SAM (prepared with 20% thiol azide) bearing 56 pmol.cm^{-2} peptide.

SPR binding assays were then carried out to determine the kinetic parameters of the RTX-CD20 interaction as a function of CD20 surface density. Figure 3 depicts the recorded binding response profiles for three different CD20 surface densities. The sensorgram shapes along with the magnitude of the equilibrium responses show a dependence of RTX binding on the ligand density in the following rank order: 46 > 2.8 > 85 pmol.cm^{-2}. Figure 3B shows a saturation for the SPR signal at 500 nM (2000 RU) while for 2.8 pmol.cm^{-2} (Fig. 3A) and 85 pmol.cm^{-2} (Fig. 3C) the SPR responses did not reach the saturation (1000 RU and 450 RU for 1 µM, respectively). It is important to note that for the highest CD20 surface density the

affinity is the lowest. An enhancement of the affinity with the increase of the CD20 surface density until reaching a plateau was expected.

The so-called heterogeneous ligand (HL) model was used to extract kinetic parameters, i.e. the on-rate (k_{on}) and off-rate (k_{off}), from the data (Fig. S6-S7, table S1, in the supporting information). This model allows interactions with up to two ligand species with distinct kinetic parameters. The deconvolution of the modeled curves revealed that one interaction was generally dominant. The second interaction exhibited low magnitude, and the shape of the curves (for the second interaction) was characteristic of a non-specific interaction. We hypothesize that the second interaction is related to soluble RTX aggregates which can interact with CD20 surface, as self-association of RTX has been already mentioned in the literature.[27] The fitted data based on the HL model are presented on the sensorgrams in figure 3 for the association and dissociation phases corresponding to the mAb interaction. The apparent K_D determined either by using the kinetic data (k_{off}/k_{on} ratio) or by a Langmuir binding isotherm plotted from the sensorgrams at steady-state equilibrium are similar (Table 2).

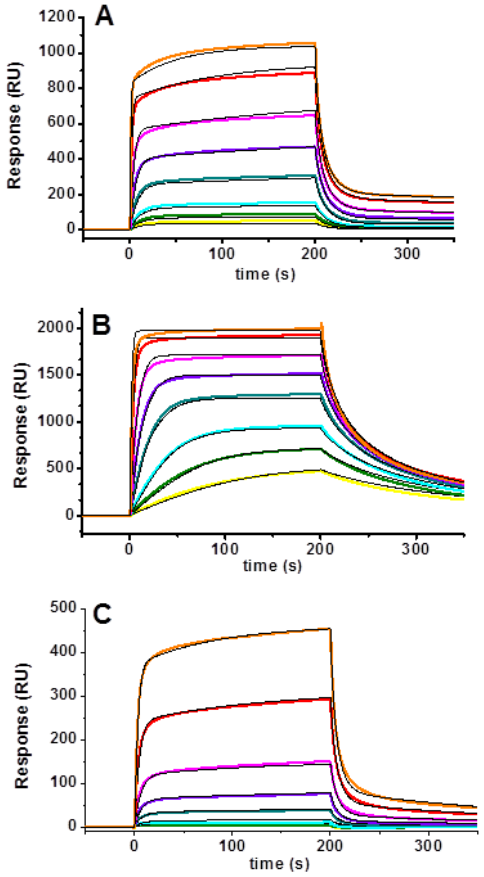

Figure 3. RTX-CD20 SPR binding profiles. Sensorgrams were recorded at different CD20 surface densities: (A) 2.8 pmol.cm^{-2}, (B) 46 pmol.cm^{-2}, and (C) 85 pmol.cm^{-2}. RTX concentrations were ranging from 5 to 1000 nM (5, 10, 20, 50, 100, 200, 500 and 1000 from yellow to orange curves). The sensorgrams were fitted with the heterogeneous ligand kinetic model (RI correction = 0) and the fitted curves were added to the graph (black curves).

Figure 4A depicts the evolution of these apparent K_D values as a function of CD20 surface density. It clearly shows a dependence of the ligand density on the RTX binding affinity. At low antigen density (2.1 pmol.cm^{-2}), the K_D value is extremely high (977 ± 8 nM). When increasing the CD20 densities, the K_D values decrease until reaching a minimum of 32 nM for a surface displaying around 46 pmol.cm^{-2} of CD20 epitope, which appears to be the optimal surface density. Interestingly, the apparent maximum response obtained at 46 pmol.cm^{-2} CD20 (K_D = 32 nM) is close to the values reported from *in vitro* analysis performed by flow cytometry with CD20-expressing cells (5-19 nM).[8,9] Increasing the CD20 epitope density beyond 46 pmol.cm^{-2} to 85 pmol.cm^{-2}, was accompanied by a dramatic increase of K_D to values in the micromolar range. Such evolution can be rationalized by the influence of the average inter-antigen distance on the RTX binding affinity on the antigenic surface. Compactness of the CD20 layer is expected when the inter-antigen distance decreases. Correlating with the K_D evolution, we observe an inverse variation of the maximum SPR responses (R_{max} values) as shown the figure 4B. The maximum binding capacity of RTX is observed for 46 pmol.cm^{-2} (corresponding to the minimal K_D), whereas R_{max} values fall down afterwards, meaning that less mAbs interact with the surface at high surface density. This result can be assigned to the high compactness of the layer due to CD20-CD20 interaction that makes the CD20 epitope less available for RTX binding.

By using a previously reported model,[28,29] we were able to estimate the fraction of surface-grafted antigens that is available for RTX binding. Based on consideration of antibody size and antigen surface density, CD20 epitopes already engaged in RTX interaction or effectively obstructed by a surrounding RTX were excluded to estimate the fraction of antigens accessible for additional binding (Fig. S13, Eqs. S4-5, in the supporting information). For a CD20 density of 46 pmol.cm^{-2}, only 20% of CD20 are available for a subsequent RTX rebinding (Fig. S13 in the supporting information). Under this circumstance, the R_{max} cannot be enhanced further above a grafting density of 50-60 pmol.cm^{-2}. Furthermore, high densities of CD20 could generate CD20-CD20 interaction that inhibits the binding of mAb.

In addition to SPR analysis, an apparent binding affinity was determined by QCM-D (Table S2, Eq. S6, Fig. S14 in the supporting information) from the shift in frequency measured for various RTX concentrations on surfaces displaying 2.8, 46 and 85 pmol.cm^{-2} of CD20 epitope. As expected, similar results were observed and a minimal K_D was obtained for 46 pmol.cm^{-2} (Table S2 in the supporting information).

Furthermore, K_D-related observations can be made for kinetic parameters, especially for k_{on} values that tend to follow similar variation. Table 2 shows a 10-fold increase in k_{on} for CD20 densities between 2.1 pmol.cm^{-2} (4.7×10^5 M^{-1}.s^{-1}) and 23.7 pmol.cm^{-2} (45.6×10^5 M^{-1}.s^{-1}). This density range corresponds to the growth of available CD20-containing surface densities until reaching a plateau corresponding to 46 pmol.cm^{-2} (Fig. S7 in the supporting information). Values of k_{on} increase with the amount of antigens on the surface, while K_D values decrease. In contrast, for high CD20 densities (Γ_{CD20} > 46 pmol.cm^{-2}), the drop in k_{on} is explained by CD20-CD20 interaction on surface that reduces their accessibility. Such results have already been reported in the literature.[30]

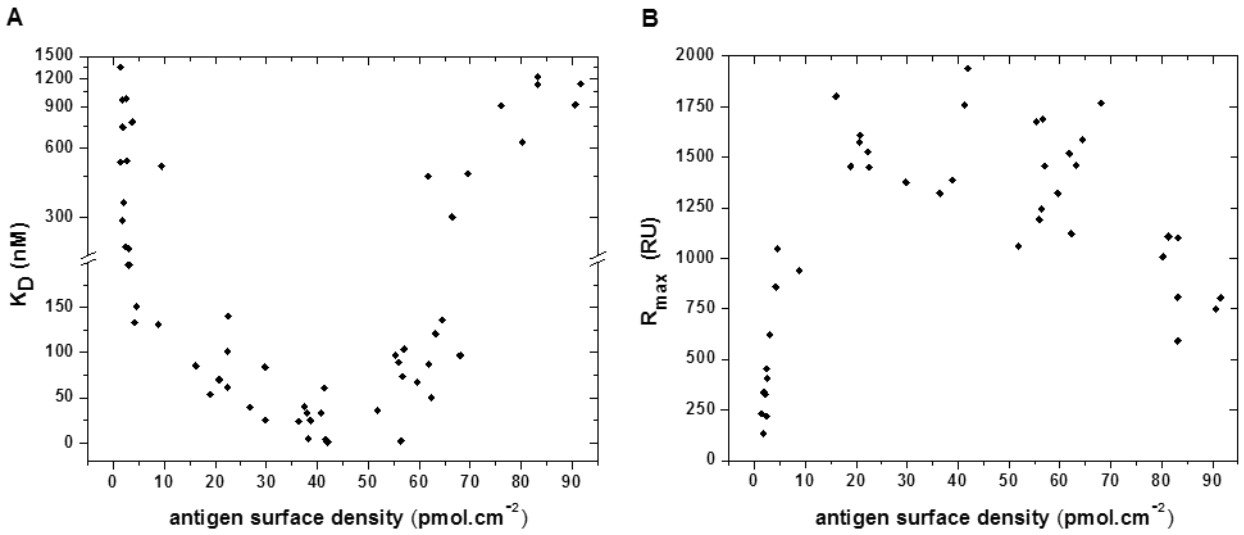

Figure 4. Impact of CD20 density on RTX binding affinity. (A) Binding affinity, (B) R_{max} measured for RTX (K_D and R_{max} were determined by kinetic data). The antigen surface density was calculated with Jung's formula, starting from the resonance response unit (RU) corresponding to the *in situ* covalent grafting of CD20 epitope to the sensor chips.

Table 2. Inter-antigen spacing, kinetic and thermodynamic parameters for CD20 / RTX binding as a function of CD20 surface density.

N_3 (%)	Γ_{CD20} (pmol.cm^{-2}) [a]	Inter-antigen spacing (nm) [b]	k_{on} (RTX) (10^5 M^{-1}.s^{-1})	k_{off} (RTX) (s^{-1})	K_D (Kinetic) (nM)	K_D (Steady-state) (nM)
0.1	2.1 ± 0.4	9.1 ± 0.8	4.7 ± 1.3	0.46 ± 0.02	977 ± 8	694 ± 37
1	2.8 ± 0.8	7.4 ± 1.2	17.7 ± 7.1	0.46 ± 0.24	248 ± 94	273 ± 72
2.5	23.7 ± 4.0	2.7 ± 0.2	45.6 ± 6.8	0.35 ± 0.07	75 ± 6	98 ± 9
12.5	46.1 ± 10.5	2.0 ± 0.2	27.5 ± 9.3	0.08 ± 0.03	32 ± 12	25 ± 12
20	56.0 ± 13.0	1.8 ± 0.2	17.3 ± 2.2	0.27 ± 0.06	152 ± 16	181 ± 16
50	84.9 ± 4.9	1.4 ± 0.0	4.4 ± 2.6	0.47 ± 0.32	1007 ± 16	1156 ± 114

(a) CD20 Surface density on SPR sensor chip determined by Jung's formula. (b) Root-mean-square distances between two CD20 epitopes calculated from the surface densities.

Concurrently, values of k_{off} decrease significantly with increasing densities until a minimal value (k_{off} = 0.08 s^{-1}) at 46 pmol.cm^{-2}. For high CD20 densities, values of k_{off} increase to about 0.4 s^{-1} (Table 2).

All these variations are consistent with a high probability of a statistical rebinding of the mAb together with the occurrence of potential bivalent binding when CD20 density reaches an optimal value with sufficient inter-antigen distance while maintaining good accessibility of the antigen (Fig. 5). These two phenomena cannot be discriminated using SPR. This technique measures the change in the refractive index near the surface. The change in refractive index is proportional to the total amount of RTX in close proximity to the surface but cannot discriminate those which are bound by one arm to those bound by two arms.

The effect of antigen surface density on the binding affinity of antibodies has been already reported in the literature, for instance for HIV-1 neutralizing antibodies interacting with gp120 glycoprotein.[31] The data reveal that the extent of the changes of the binding energetics as a function of antigen density strongly depend on the binding affinity of each antibody. The authors observed a marked increase in avidity to variation in antigen density in the case of low to moderate binding affinity whereas the impact of antigen immobilization is very low for antibodies exhibiting high affinity.

To better understand the gain of affinity due to the statistical rebinding and to the bivalency of the mAb, RTX Fab fragments were used for SPR binding assays (Fig. S15, in the supporting information). Table 3 shows the kinetic parameters obtained for the Fab on surfaces displaying 2.8 and 46 pmol.cm^{-2} of CD20. We observe that k_{on} and k_{off} values are affected when increasing the CD20 surface density. These concomitant variations are supported by the change in accessibility of CD20 epitope which is dependent on the CD20 surface density resulting in a significant increase of K_D (12700 *vs* 617 nM, for 2.8 and 46 pmol.cm^{-2} of CD20 respectively). Interestingly, the k_{off} value for the Fab (0.64 x 10^5 M^{-1}.s^{-1}) is similar to the one obtained for RTX (0.46 x 10^5 M^{-1}.s^{-1}) for surface displaying 2.8 pmol.cm^{-2} of CD20. This result suggests that statistical rebinding is restricted on surface displaying low CD20 density (Figure 5). On the contrary, the rate of association for the Fab is around 30-fold lower than for the bivalent mAb (0.6 *vs* 17.7 x 10^5 M^{-1}.s^{-1}) (See Fig S16, in the supporting information). Such discrepancies can be explained by the bivalency of the RTX/CD20 interaction and the flexibility of the two Fab arms (3-14 nm) that would allow the mAb a wider search range for CD20 binding sites compared to Fab. The

enhancement of avidity afforded by the bivalency of RTX is more pronounced for a CD20 surface density of 2.8 pmol.cm^{-2}. Consequently, k_{on} is greatly affected by these phenomena. Such comparison underlines the bivalency effect for the association of RTX when antigen density is low. For surface density of 46 pmol.cm^{-2} of CD20, the k_{off} values for the Fab (0.2 s^{-1}) and for the RTX (0.08 s^{-1}) point out the high probability of RTX rebinding on CD20 surface. Intrinsic flexibility of the mAb allows exploring large surface as the distance between both active sites (paratope) varies from 3 to 14 nm.[32] Together these results show how important is the role of the second arm on the RTX binding capacities, as it improves the affinity of the mAb for the surface and its statistical rebinding (Figure 5). Regarding the K_D values, a strong difference is observed for 2.8 pmol.cm^{-2} (K_D = 12700 nM for Fab *vs* K_D = 248 nM for RTX) and, to a lesser extent, for 46 pmol.cm^{-2} (K_D = 617 nM for Fab *vs* K_D = 32 nM for RTX), leading to Fab/RTX K_D ratios of 51 and 19 respectively. These data are in accordance with values from the literature. Whitesides et al. reported a 50-fold enhancement of binding for a synthetic bivalent protein dimer (mimicking mAb) compared to the monovalent one interacting with mixed SAMs presenting ligands.[33] It is worth noting that the contribution of the surface densities can be isolated by comparing the K_D values related to RTX Fab - CD20 interaction at 2 and 46 pmol.cm^{-2}. It turns out that a 21-fold factor is observed from low to medium antigen grafting density. As RTX Fab is a monovalent molecule, improvement of affinity is exclusively due to surface densities, improving the rate of association, and the rate of dissociation via rebinding process. We have to underline that this phenomenon also exists for the mAb-CD20 recognition but to a lesser extent, 7-fold factor (K_D = 248 nM for density of 2.8 pmol.cm^{-2} *vs* 32 nM for 46.1 pmol.cm^{-2}). This result confirms that the contribution of bivalency is critical for both the mAb association, but also for the statistical rebinding. The rebinding process was described by Preiner et al. as a stochastic walking of IgGs on 2D rigid surfaces.[34] The authors demonstrated by high speed atomic force microscopy that the moving speeds and step sizes are dependent of the antigen density.

Table 3. Kinetic parameters for the CD20 / RTX Fab binding.

N_3 (%)	Γ_{CD20} (pmol.cm^{-2}) [a]	k_{on} (RTX Fab) (10^5 M^{-1}.s^{-1})	k_{off} (RTX Fab) (s^{-1})	K_D (Kinetic) (nM)
1	2.8 ± 0.8	0.6 ± 0.2	0.64 ± 0.12	12700 ± 3750
12.5	46.1 ± 10.5	3.8 ± 0.8	0.2 ± 0.02	617 ± 74

(a) CD20 Surface density on SPR sensor chip determined by Jung's formula.

To date, there is evidence supporting the impact of CD20 distribution on the clinical efficacies of RTX.[6,7,35] Antigen density is a critical parameter that determines the biological efficacy of the mAb especially *via* the complement-induced cell death. Additionally, microscopy experiments of fluorescent RTX showed a heterogeneous distribution of CD20 antigens on the cell surface,[8] suggesting that CD20 proteins are organized into clusters.[36] In our study, the highest affinity was determined for a CD20 surface density of 46 pmol.cm^{-2} which corresponds to an average inter-antigen spacing of around 2 nm (Table 2). Considering the size of CD20-expressing B cells (around 8 µm in diameter) and the amount of CD20 antigens per cells (2 to 6 × 10^5),[5,8,37] a homogeneous distribution would imply areal mass densities of 0.003 to 0.6 pmol.cm^{-2}. According to our SPR experiments, these values (average inter-antigen spacing above 7 nm) correspond to surfaces that did not allow strong RTX binding (Fig. 5, Table 2). Together, our results provide strong evidence for a nanoscale distribution of CD20 and the requirement of an average critical inter-antigen spacing of 2 nm for RTX binding. We suggest that this critical CD20 density is required within CD20 clusters on cell surface for efficient RTX binding.

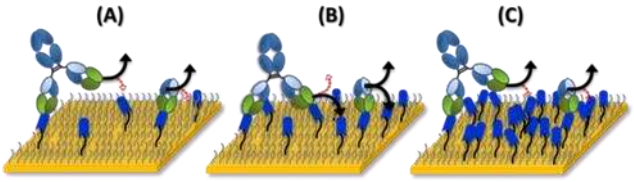

Figure 5. Schematic of rebinding phenomena occurring on surfaces displaying CD20 surface densities during the rinsing step: (A) low, (B) medium, (C) high CD20 surface densities. At low and high antigen surface density, the antibody is mostly bound through one arm like the Fab, and is quickly removed from the surface (A and C). At medium antigen surface density (46 pmol.cm^{-2}), the probability of the mAb to bind with the two arms and to find a neighboring antigen after dissociation of one of its arm is high, leading to a lower k_{off}, and so a stronger avidity.

CONCLUSION

In this study, we designed surfaces with tunable areal mass densities of the CD20 epitope. We were able to study the contribution of the statistical rebinding and the bivalent effect of RTX mAb, especially through a comparison with the RTX Fab. An average critical inter-CD20 spacing of nearly 2 nm was found that confers the best conditions for RTX binding. This nanoscale distribution corroborates the prerequisite CD20 cluster formation for biological activity of RTX. It is expected that this inter-antigen spacing might be required for other mAbs as well. Additionally, we reason that the design of such surfaces will pave the way for the discovery of mAb mimics, especially through the screening of peptides, nucleic acid aptamers or phage libraries.

ASSOCIATED CONTENT

Supporting Information

Detailed description on the CD20 epitope synthesis (HPLC and mass analysis) and additional SPR sensorgrams and QCM-D profiles were available in the supporting information. The Supporting Information is available free of charge on the ACS Publications website.

AUTHOR INFORMATION

Corresponding Author

* E-mail: didier.boturyn@univ-grenoble-alpes.fr.

Present Addresses

†If an author's address is different than the one given in the affiliation line, this information may be included here.

Author Contributions

The manuscript was written through contributions of all authors. All authors have given approval to the final version of the manuscript.

ACKNOWLEDGMENT

This work was supported by the CNRS, the University Grenoble Alpes, the "Communauté d'agglomération Grenoble-Alpes Métropole" (Nanobio program) and by the "Agence Nationale de la Recherche" including "Mimobody" research support (ANR-13-BS07-0014-01) and LabEx ARCANE and CBH-EUR-GS (ANR-17-EURE-0003). Laure Bar acknowledges the "Groupe français des peptides et des protéines" (GFPP) for a grant to cover travel to Leeds for SE experiments. The authors wish to acknowledge the support from the ICMG chemistry platform, Grenoble, on which the peptide synthesis has been performed, the ICMG PCI platform, Grenoble, on which analyses were done, and Genentech, Inc. (San Francisco), a member of Roche group, for providing Rituximab.

REFERENCES

(1) Ecker, D. M.; Dana Jones, S.; Levine, H. L. The therapeutic monoclonal antibody market. *mAbs* **2015**, *7*, 9-14.
(2) Twomey, J. D.; Brahme, N. N.; Zhang, B. Drug-biomarker co-development in oncology - 20 years and counting. *Drug Resist. Update* **2017**, *30*, 48-62.
(3) Scott, A. M.; Wolchok, J. D.; Old, L. J. Antibody therapy of cancer. *Nature* **2012**, *12*, 278-287.
(4) Klein, C.; Lammens, A.; Schäfer, W.; Georges, G.; Schwaiger, M.; Mössner, E; Hopfner, K.-P.; Umaña P.; Niederfellner, G. Epitope interactions of monoclonal antibodies targeting CD20 and their relationship to functional properties. *mAbs* **2013**, *5*, 22-33.
(5) Singh, V.; Gupta, D.; Arora, R.; Tripathi, R. P.; Almasan, A.; Macklis, R. M. Surface levels of CD20 determine Aanti-CD20 antibodies mediated cell death *in vitro*. *PLoS One* **2014**, *9*, e111113. doi: 10.1371/journal.pone.0111113.
(6) Van Meerten, T.; Van Rijn, R. S.; Hol, S.; Hagenbeek, A.; Ebeling, S. B. Complement-induced cell death by rituximab depends on CD20 expression level and acts complementary to antibody-dependent cellular cytotoxicity. *Clin. Cancer Res.* **2006**, *12*, 4027-4035.
(7) Li, M.; Xiao, X.; Zhang, W.; Liu, L.; Xi, N.; Wang,, Y. Nanoscale distribution of CD20 on B-cell lymphoma tumour cells and its potential role in the clinical efficacy of rituximab. *J. Microsc.* **2014**, *254*, 19-30.
(8) Melhus, K. B.; Larsen, R. H.; Stokke, T.; Kaalhus, O; Selbo, P. K.; Dahle, J. Evaluation of the binding of radiolabeled rituximab to CD20-positive lymphoma cells: an *in vitro* feasibility study concerning low-dose-rate radioimmunotherapy with the α-emitter ^{227Th}. *Cancer Biother. Radiopharm* **2007**, *22*, 469-479.
(9) Reff, M. E.; Carner, K.; Chambers, K. S.; Chinn, P. C.; Leonard, J. E.; Raab, R..; Newman, R. A.; Hanna, N.; Anderson, D. R. Depletion of B cells in vivo by a chimeric mouse human monoclonal antibody to CD20. *Blood* **1994**, *83*, 435-445.
(10) Blasco, H.; Lalmanach, G. ; Godat, E. ; Maurel, M.C. ; Canepa, S. ; Belghazi, M. ; Paintaud, G. ; Degenne, D. ; Chatelut, E. ; Cartron, G. ; Le Guellec, C. Evaluation of a peptide ELISA for the detection of rituximab in serum. *J. Immunol. Methods* **2007**, *325*, 127-139.
(11) Liu, J. L.; Zabetakis, D.; Goldman, E. R.; Anderson, G. P. Selection and characterization of single domain antibodies against human CD20. *Mol. Immunol.* **2016**, *78*, 146-154.
(12) Gori, A.; Longhi. R. *Peptide Microarrays: Methods and Protocols* (eds. Cretich, M. & Chiari, M.) **2016**, 145–156.
(13) Puiu, M.; Bala, C. Peptide-based biosensors: From self-assembled interfaces to molecular probes in electrochemical assays. *Bioelectrochemistry* **2018**, 120, 66–75.
(14) Puiu, M.; Bala, C. Building switchable peptide-architectures on gold/composite surfaces: New perspectives in electrochemical bioassays. *Curr. Opin. in Electrochemistry* **2018**, *12*, 13-20.
(15) Leo, N.; Liu, J.; Archbold, I. ; Tang, Y.; Zeng, X. Ionic strength, surface charge, and packing density effects on the properties of peptide self-assembled monolayers. *Langmuir* **2017**, *33*, 2050–2058.
(16) Hudalla, G. A.; Murphy, W. L. Using "Click" chemistry to prepare SAM substrates to study stem cell adhesion. *Langmuir* **2009**, *25*, 5737–5746.
(17) Gerasimov, J. Y.; Lai, R. Y. Design and characterization of an electrochemical peptide-based sensor fabricated via "click" chemistry. *Chem. Commun.* **2011**, *47*, 8688–8690.
(18) Gori, A.; Cretich, M.; Vanna, R.; Sola, L. ; Gagni, P.; Bruni, G.; Liprino, M.; Gramatica, F.; Burastero, S.; Chiari, M. Multiple epitope presentation and surface density control enabled by chemoselective immobilization lead to enhanced performance in IgE-binding fingerprinting on peptide microarrays. *Anal. Chim. Acta* **2017**, *983*, 189-197.
(19) Raigoza, A. F.; Onyirioha, K.; Webb, L. J. Controlling noncovalent interactions between a lysine-rich α-helical peptide and self-assembled monolayers of alkanethiols on Au through functional group diversity. *Appl. Surf. Sc.* **2017**, 396, 1831-1839.
(20) Du, J.; Wang, H.; Zhong, C.; Peng, B.; Zhang, M.; Li, B.; Huo, S.; Guo, Y.; Ding, J. Structural basis for recognition of CD20 by therapeutic antibody rituximab. *J. Biol. Chem.* **2007**, *282*, 15073-15080.
(21) Degardin, M.; Thakar, D.; Claron, M.; Richter, R. P.; Coche-Guérente, L.; Boturyn, D. Development of a selective cell capture and release assay: impact of clustered RGD ligands. *J. Mater. Chem. B* **2017**, *5*, 4745-4753.
(22) Dubacheva, G. V.; Van Der Heyden, A.; Dumy, P.; Kaftan, O.; Auzély-Velty, R.; Coche-Guerente, L.; Labbé, P. Electrochemically controlled adsorption of Fc-functionalized polymers on β-CD-modified self-assembled monolayers. *Langmuir* **2010**, *26*, 13976–13986.
(23) Prime, K. L.; Whitesides, G. M. Adsorption of proteins onto surfaces containing end-attached oligo(ethylene oxide): a model system using self-assembled monolayers. *J. Am. Chem. Soc.* **1993**, *115*, 10714-10721.
(24) Ta, D. T.; Guedens, W.; Vranken, T.; Vanschoenbeek, K; Redeker, E. S.; Michiels, L.; Adriaensens, P. Enhanced biosensor platforms for detecting the atherosclerotic biomarker VCAM1 Bbased on bioconjugation with uniformly oriented VCAM1-targeting nanobodies. *Biosensors* **2016**, *6*, 34. doi: 10.3390/bios6030034.
(25) Solano, I.; Parisse, P.; Gramazio, F.; Cavalleri, O.; Bracco, G.; Castronovo, M.; Casalis, L. ; Canepa, M. Spectroscopic ellipsometry meets AFM nanolithography: about hydration of bio-inert oligo(ethylene glycol)-terminated self assembled monolayers on gold. *Phys. Chem. Chem. Phys.* **2015**, *17*, 28774-28781.
(26) Bingen, P.; Wang, G.; Steinmetz, N. F.; Rodahl, M.; Richter, R. P. Solvation effects in the quartz crystal microbalance with dissipation monitoring response to biomolecular adsorption. A phenomenological approach. *Anal. Chem.* **2008**, *80*, 8880-8890.
(27) Morgan, H.; Tseng, S.-Y.; Gallais, Y.; Leineweber, M.; Buchmann,V.; Riccardi, S.; Nabhan, M.; Lo, J.; Gani, Z.; Szely, N.; Zhu, C. S.; Yang, M.; Kiessling, A.; Vohr, H.-W.; Pallardy, M.; Aswad, F.; Turbica, I. Evaluation of *in vitro* assays to assess the modulation of dendritic cells functions by therapeutic antibodies and aggregates. *Front. Immunol.* **2019**, 10: 601. doi: 10.3389/fimmu.2019.00601.
(28) Yang, T.; Baryshnikova, O. K.; Mao, H.; Holden, M. A.; Cremer, P. S. Investigations of bivalent antibody binding on fluid-supported phospholipid membranes: the effect of hapten density. *J. Am. Chem. Soc.* **2003**, *125*, 4779-4784.
(29) Hlavacek, W. S.; Posner, R. G.; Perelson, A. S. Steric effects on multivalent ligand-receptor binding: exclusion of ligand sites by bound cell surface receptors. *Biophys. J.* **1999**, *76*, 3031-3043.
(30) Jung, H.; Robison, A. D.; Cremer, P. S. Multivalent ligand-receptor binding on supported lipid bilayers. *J. Struct. Biol.* **2009**, *168*, 90-94.
(31) Hadzhieva, M.; Pashov, A. D.; Kaveri, S.; Lacroix-Desmazes, S.; Mouquet, H.; Dimitrov, J. D. Impact of antigen density on the binding mechanism of IgG antibodies. *Sci. Rep.* **2017**, *7*, 3767. doi: 10.1038/s41598-017-03942-z.
(32) Galanti, M.; Fanelli, D.; Piazza, F. Conformation-controlled binding kinetics of antibodies. *Sci. Rep.* **2016**, *6*, 18976. doi: 10.1038/srep18976.
(33) Mack, E. T.; Snyder, P. W.; Perez-Castillejos, R.; Whitesides, G. M. Using covalent dimers of human carbonic anhydrase II to model bivalency in immunoglobulins. *J. Am. Chem. Soc.* **2011**, *133*, 11701–11715.

(34) Preiner, J.; Kodera, N.; Tang, J.; Ebner, A.; Brameshuber, M.; Blaas, D.; Gelbmann, N.; Gruber, H. J.; Ando, T.; Hinterdorfer, P. IgGs are made for walking on bacterial and viral surfaces. *Nat. Commun.* **2014**, *5*: 4394. doi: 10.1038/ncomms5394.
(35) Huh, Y. O.; Keating, M. J.; Saffer, H. L.; Jilani, I.; Lerner, S.; Albitar M. Higher levels of surface CD20 expression on circulating lymphocytes compared with bone marrow and lymph nodes in B-cell chronic lymphocytic leukemia. *Am. J. Clin. Pathol,* **2001**, *116*, 437-443.
(36) Cartron, G.; Watier, H.; Golay, J.; Solal-Celigny, P. From the bench to the bedside: ways to improve rituximab efficacy. *Blood* **2004**, *104*, 2635-2642.
(37) Ward, E.; Mittereder, N.; Kuta, E.; Sims, G. P.; Bowen, M. A.; Dall'Acqua, W.; Tedder, T.; Kiener, P.; Coyle, A. J.; Wu, H.; Jallal, B.; Herbst, R A glycoengineered anti-CD19 antibody with potent antibody-dependent cellular cytotoxicity activity *in vitro* and lymphoma growth inhibition *in vivo*. *Br. J. Haematol.* **2011**, *155*, 426–437.

SUPPORTING INFORMATION

Impact of antigen density on recognition by monoclonal antibodies

Laure Bar,[†] Jérôme Dejeu,[†] Rémy Lartia,[†] Fouzia Bano,[‡] Ralf P. Richter,[‡] Liliane Coche-Guérente[*†] and Didier Boturyn[*†]

[†]Univ. Grenoble-Alpes, CNRS, DCM UMR 5250, F-38000 Grenoble, France

[‡]University of Leeds, School of Biomedical Sciences, Faculty of Biological Sciences, School of Physics and Astronomy, Faculty of Engineering and Physical Sciences, Astbury Center for Structural Molecular Biology, and Bragg Centre for Materials Research, Leeds, United Kingdom

Corresponding Author:

[*] E-mail: didier.boturyn@univ-grenoble-alpes.fr.

Table of Contents:

1. General procedure for CD20 synthesis

1.1. Reagents and material

All Fmoc amino acid derivatives and resins were purchased from Advanced ChemTech Europe (Brussels, Belgium), Bachem Biochimie SARL (Voisins-Les-Bretonneux, France) and France Biochem S.A. (Meudon, France). Other reagents were obtained from Aldrich (Saint Quentin Fallavier, France) or Acros (Noisy-Le-Grand, France). RP-UHPLC analyses were performed on Waters equipment consisting of a Waters Acquity H-Class Bio UPLC combined to a Waters SQ Detector 2 mass spectrometer. The analytical column used was a ACQUITY UPLC BEH C18 Column, 130Å, 1.7 µm, 2.1 mm x 50 mm operated at 0.6 mL/min with linear gradient programs in 2.20 min run time (routine program: 5% to 100 % B in 2.20 min). UV monitoring was performed at 214 nm. Solvent A consisted of H2O containing 0.1% trifluoroacetic acid (TFA) and solvent B consisted of CH3CN containing 0.1% TFA. Water was of Milli-Q quality. CH3CN and TFA were LC-MS grade. RP-HPLC purifications were performed on Gilson GX-281 or GX-281. The preparative column, Macherey-Nagel 100 Å 7 µm C18 particles, 250 × 21 mm was operated at 20.84 mL/min. Solvents A and B were the same as the ones used in RP-HPLC analysis.

1.2. Synthesis of CD20

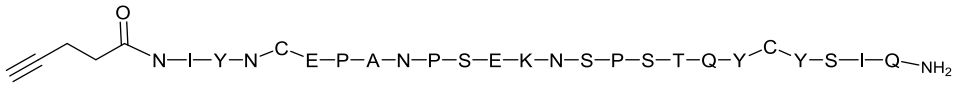

Synthesis of the protected peptide was carried out using the Fmoc/*t*-Bu strategy. For both peptides, the first amino-acid was manually attached on a 2-chlorotritylchloride® resin (loading ≈ 0.5 mmol/g). Peptides were then elongated on a peptide synthesizer. Coupling reactions were performed by using 4 eq. of *N*-Fmoc-protected amino acid (relative to the resin loading) activated *in situ* with 2 equiv. of HBTU and 3-5 eq. of diisopropylethylamine (DIPEA) in DMF (10 mL/g resin) for 30 min. *N*-Fmoc protecting groups were removed by treatment with a piperidine/DMF solution (1:4) for 10 min (10 mL/g resin). The alkyne function was then manually added on N-terminus by a coupling reaction with 4-Pentynoic acid (2 equiv.). The linear peptides were then released from the resin by treatments with a solution of trifluoroacetic acid/trisisopropylsilane/H_2O/2,2′-(Ethylenedioxy)diethanethiol (92.5/2.5/2.5/2.5, 10 mL/mg resin, 1 h). With this treatment, all protecting group of the peptides are removed. After evaporation, diethyl ether was added to precipitate peptides. They were then triturated and washed three times with diethyl ether to obtain crude materials.

1.3. Disulfide bond formation

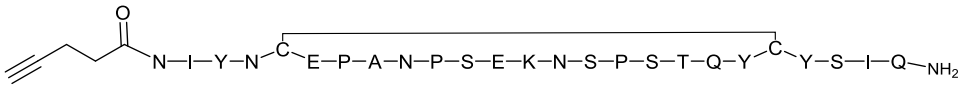

Disulfide bonds were formed by diluting peptides to 500 µM in Tris buffer 0.1 M, guanidine 20 mM, and DMSO 5% (v:v) and maintaining oxidative conditions for 48 h. Disulfide bond formation was checked by RP-UHPLC analyses.

Peptides were then purified by RP-HPLC and their concentration quantified with a UV spectrophotometer.

UPLC analysis of CD20:

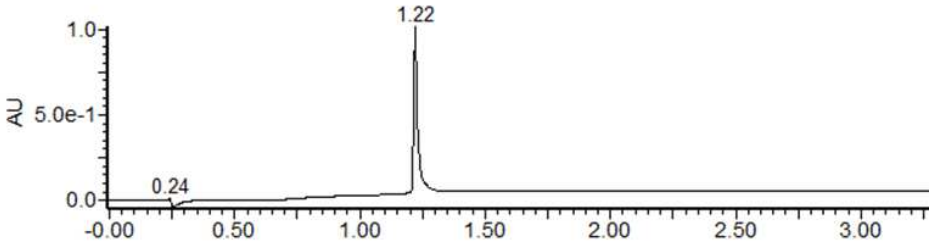

ESI analysis of CD20:

MS (ESI-MS, positive mode): $C_{126}H_{183}N_{33}O_{44}S_2$ Calcd : MW = 2928.264 g.mol^{-1} ; Found MW = 2928.22 g.mol^{-1}

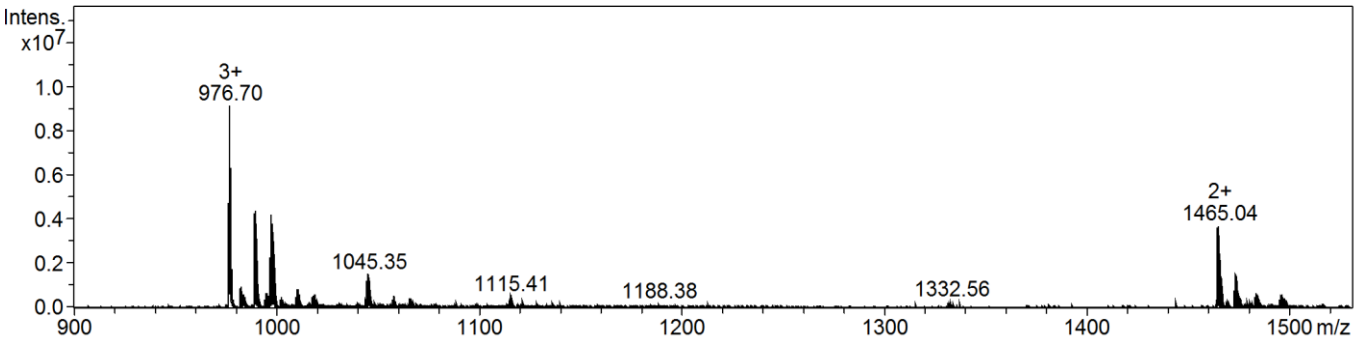

2. SPR quantification of grafted peptide

2.1. Jung's formula

Surface Plasmon resonance (SPR) is an optical sensing technique which, similar to SE, is sensitive to changes in refractive index. We considered here a multilayer structure with the first layer SAM used to subsequently attach CD20 epitope considered as a second layer that has been monitored by SPR. The Jung's formula [1] combined with the De Feijter's equation (Eq. S1) allowed the conversion of the magnitude of the response units measured during the chemical coupling (conventionally expressed in RU) into areal mass densities Γ (in mol.cm^{-2}) as previously reported (Eq. S1): [2]

$$\Gamma = 10^{-6} RU . \frac{d'}{dn/dc} \frac{1}{e^{-d/dp}\left(1 - e^{-d'/dp}\right)} \quad \text{(Eq. S1)}$$

where RU is the number of resonance units gained by the peptide grafting, d' is the thickness of the peptide film (d' = 4.6 nm, as determined by SE), d is the thickness of the SAM (d = 2.5 nm, as determined by SE), dn/dc is the refractive index increment (*dn*/*dc* = 527 cm^3.mol^{-1} which corresponds to 0.18 x 2928 for CD20), and *dp* is the evanescent wave depth (*dp* = 175 nm).[3]

This expression requires knowledge of SAM and CD20 layer thicknesses. The SPR response would be the same as that of the simple case of a CD20 layer alone directly attached to gold surface, except that its magnitude is reduced by a factor e^{-d/d_p} due to the SAM underlayer. As the thickness of the SAM is very thin compared to the penetration depth (2.5 nm versus 175 nm), this factor is close to 1 and the response due to the attachment of the CD20 layer is unaffected by the presence of SAM layer between the metal and the CD20 layer.

2.2. SPR determination of CD20 epitope density

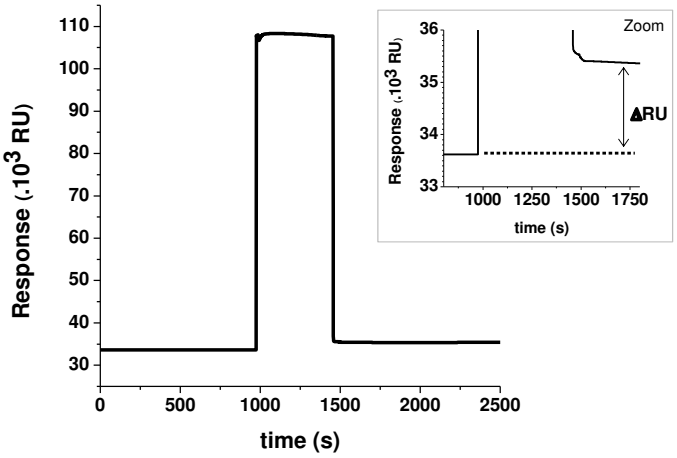

Figure S1. Determination of the number of resonance response units gained by the peptide grafting. The large change of refractive index during the injection of DMSO prevents the grafting to be monitoring in real-time. Therefore, the quantity of antigen immobilized on the surface is evaluated from the shift in resonance units after rinsing as compared to before peptide injection (ΔRU in the inset). On this example, the peptide was injected at 2 µl.min^{-1} for 480 s on a 20%-N_3 functionalized surface.

2.3. Correlation between the molar fraction of thiol-azide in the solution from which the SAMs were formed and the CD20 surface density.

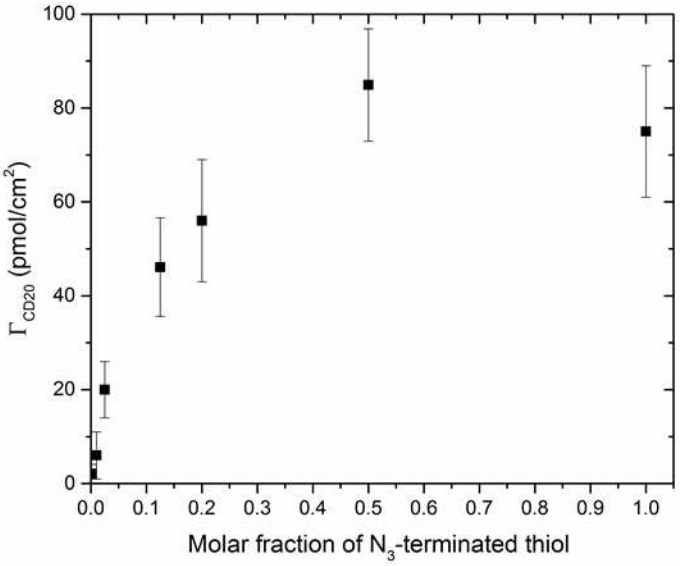

Figure S2. CD20 surface density (measured by the Jung's formula from SPR *in-situ* grafting) as a function of the molar fraction of N_3-terminated thiol in the thiol mixture used to prepare the SAMs.

Figure S2 shows that above 50% of thiol-azide CD20 surface density reached saturation. This observation could be explained by the size of CD20 (width max: 1.5 nm; length: 2.5 nm (non-stretched)). The theoretical saturation could be calculated from a densly packed layer of CD20 whose projected surface would be of 2.25 nm^2, such calculation leads to about 74 pmol/cm^2.

.

3. Optimization of SPR binding assays: Impact of buffer nature

The effect of buffer type on RTX binding to CD20 was studied since the rituximab is stored in an injectable rituximab solution (MabThera solution) that differs from the buffers we use routinely for SPR experiments. Binding assays were performed and compared in three buffer conditions (MabThera buffer, PBS buffer, or HEPES buffer) on the same surface. As can be seen on Figure S3, conventional buffers such as PBS or HEPES provided a better interaction. Consequently, we choose to work with PBS buffer after verifying the absence of dilution effect of MabThera buffer for the observed concentration range. A solution of 1 µM was prepared by diluting the RTX concentrated solution (MabThera solution of 69.5 µM) using 14.4 µL in 1000 µL of PBS.

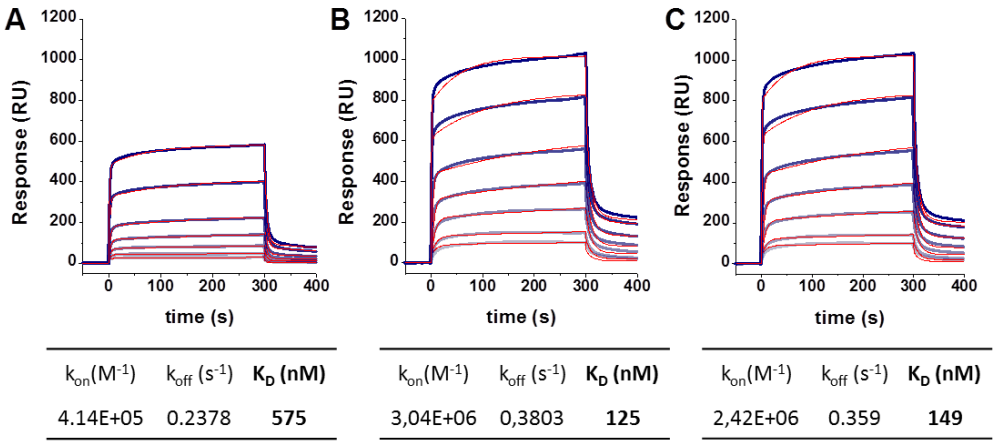

	$k_{on}(M^{-1})$	$k_{off}(s^{-1})$	K_D (nM)
A	4.14E+05	0.2378	**575**
B	3,04E+06	0,3803	**125**
C	2,42E+06	0.359	**149**

Figure S3. Binding assays performed by injecting rituximab antibody in different buffers. (A) in MabThera® Buffer = 154 mM NaCl, 25 mM citrate, 0.066% P80; (B) in PBS, 3 mM citrate, 0.005% P80; (C) in 10 mM Hepes, 150 mM NaCl, 3 mM citrate, 0.005% P80. Concentration range is: 10, 20, 50, 100, 200, 500, 1000 nM. These experiments were performed on the same surface functionalized with the ex-situ grafting protocol.

4. Specificity of CD20-functionalized surface toward RTX binding.

The graph below shows that trastuzumab (a mAb which belongs to the same IgG subclass) binds the CD20 functionalized surface in the same manner than on the CD20 scramble surface whatever the CD20 surface density.

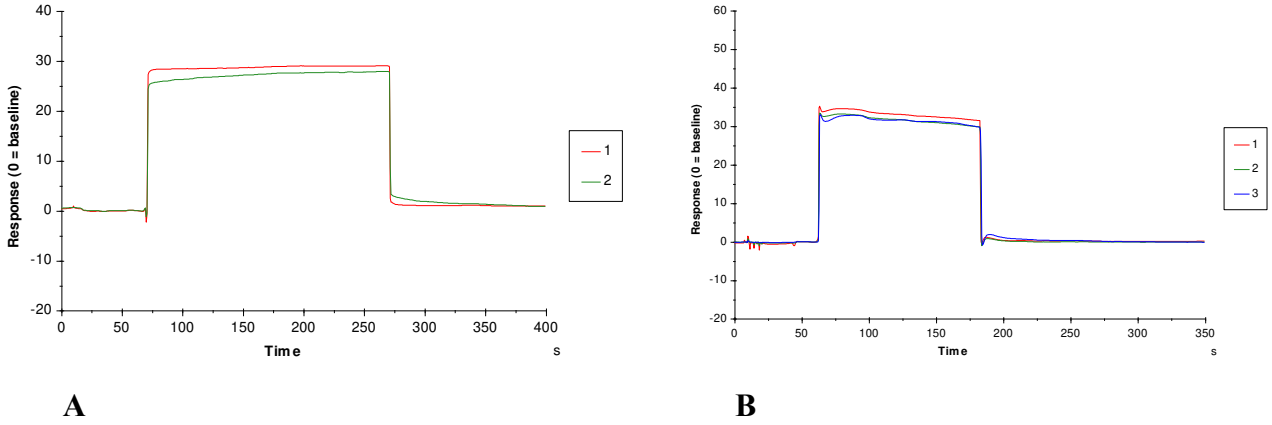

Figure S4. Overlapping of the sensorgrams characterizing the binding of trastuzumab (100 nM) on two different flow cells (Fc): Fc1 (red curve) CD20 scramble-functionalized surface, Fc2 (green curve) CD20-functionalized surface and Fc3 (blue curve) N_3-terminated SAM surface. Surface densities of CD20 or CD20 scramble functionalized surfaces correcpond to (A) 46 pmol.cm^{-2} (Fc1 and Fc2) and (B) 2.8 pmol.cm^{-2} (Fc1 and Fc2) and 0 pmol.cm^{-2} (Fc3).

Figures S4 shows that non-specific absorption of trastuzumab is similar on both CD20 and CD20 scramble surfaces at different densities.

5. Stability of the surface over time

CD20-coated SPR sensor chips were typically used for a large numbers of binding assays, each followed by a regeneration step. To confirm the stability of the CD20 coating over time, a standardized binding assay with 1 µM rituximab was performed at regular intervals. Figure S3 shows the responses corresponding to rituximab binding on a freshly prepared surface (black curve; R_{max} = 2550 RU), after 76 regeneration steps (purple curve; 2400 RU, or 94% of the initial response), and after 140 regeneration steps (blue curve; 2265 RU, or 89% of the initial response). These results confirm that the surface is stable over time, and that the loss of ligand activity was negligibly small over the duration of a binding assay.

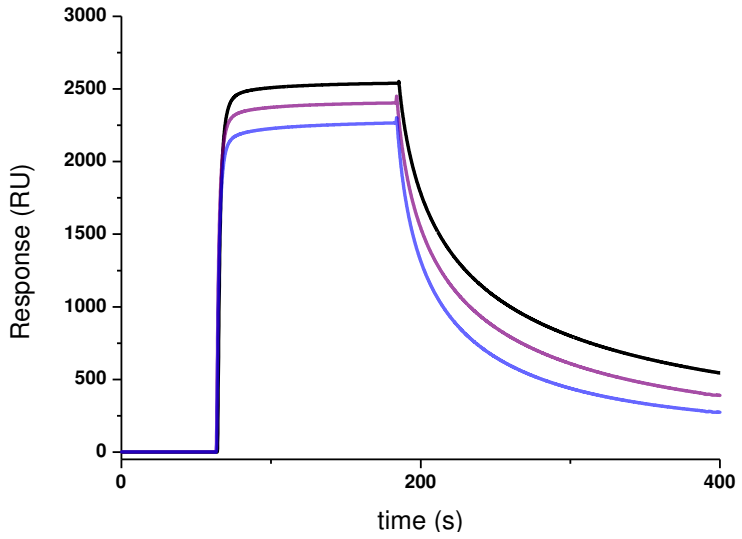

Figure S5. SPR signals obtained for a 1 µM rituximab injection on the same surface at different wear stages: freshly prepared surface (black), after 76 regeneration steps (purple), after 140 regeneration steps (blue). A regeneration step consist of an injection of Glycine/HCl solution, pH 2, for 10 s at 30 µl,min^{-1}.

6. Choice of the SPR model

The SPR data were fitted using a heterogeneous ligand (HL) model. The SPR response can be considered as a result of the contribution of two different independent interactions. One example of the deconvolution of the modelled signal is shown in figure S4. It appears that the two interactions exhibit very different magnitude, the second one is very weak and the curve shape is characteristic of a non-specific interaction with a continuous positive drift during the association phase without apparent dissociation phase. For the HL model, the data evaluation software provides two association rate constants, k_{on1} and k_{on2}, and two dissociation rate constants, k_{off1} and k_{off2}, as well as two theoretical maximal responses, R_{max1} and R_{max2}. These sets of parameters consist of the specific interaction (1st interaction in Figure S6; typically representing between 80 and 90% of the total SPR signal, see Figure S7A) and a non-specific interaction (2nd interaction in Fig. S6; representing the remaining signal of less than 20% in most cases). Consequently, the data presented in the manuscript are only related to the specific first interaction.

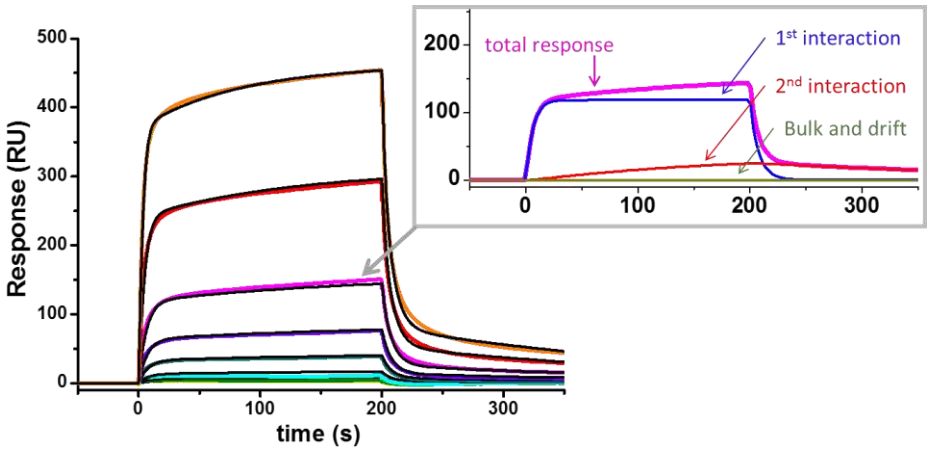

Figure S6. RTX-CD20 SPR binding profile obtained at 85 pmol.cm^{-2} of CD20 surface density. RTX concentrations were 5, 10, 20, 50, 100, 200, 500 and 1000 nM. The sensorgrams were fitted with the heterogeneous ligand kinetic model and the fitted curves were added to the graph (black curves). Insert: Signal deconvolution of the curve corresponding to the RTX injection of 500 nM. The observed sensorgram (pink) is composed of signal contributions of the specific interaction (1st interaction – blue curve) and a non-specific interaction (2nd interaction – red curve). Bulk and drift (=0) is represented by the green curve. By using the heterogeneous ligand model, we assume that each curve can be divided into two contributions. The experimental response (pink curve) is composed of a large SPR signal having the shape of a specific binding (1st interaction – blue curve) and a second weak SPR signal whose shape is characteristic of a non-specific binding (2nd interaction – red curve).

For the example presented in Figure S5, the numeric contribution of each interaction is given by the fitted R_{max} values (Table S1). With R_{max1} = 804 and R_{max2} = 127 RU, the interaction associated to the blue curve represents 84 % of the SPR response, and strengthens the idea that this corresponds to the specific interaction.

Table S1. Parameters of the CD20/RTX interaction obtained after curve fitting. The heterogeneous ligand model provides two sets of data corresponding to interaction 1 (blue curve) and interaction 2 (red curve).

k_{on1} (1/Ms)	k_{off1} (1/s)	K_{D1} (M)	R_{max1} (RU)	k_{on2} (1/Ms)	k_{off2} (1/s)	K_{D2} (M)	R_{max2} (RU)	RI (RU)	χ^2 (RU²)
6.72E+05	0.7668	1.14E-06	804	8263	0.003825	4.63E-07	127	0	7.66

Normalized maximal responses R_{max} of the two interactions are presented in Figure S7A. It shows that the signal magnitude of the second interaction is in the minority (in most cases, it represents less than 20% of the total signal magnitude). The association rate constants k_{on} for the two interactions as a function of CD20 surface coverage are shown in Figure S5B. kon values related to the second interaction are typically much smaller than for the first interaction, and the variation in kon2 is low across the full range of CD20 surface densities.

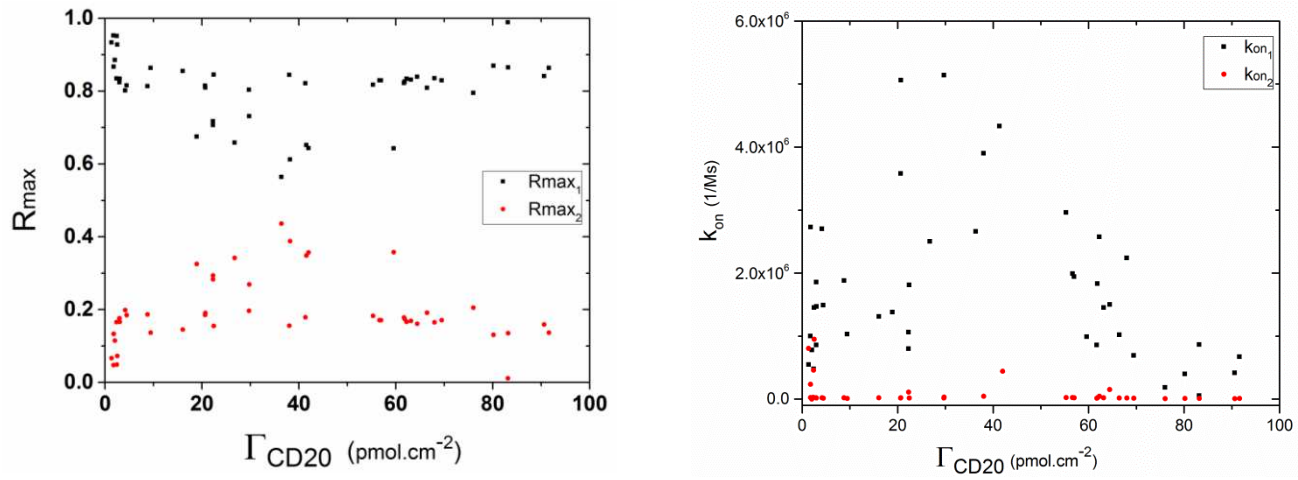

Figure S7. (A) Normalized R_{max} (for the two interactions extracted from HL model, R_{max1}: black square, R_{max2}: red disk; normalized such that $R_{max1} + R_{max2} = 1$) as a function CD20 surface coverage. (B) Association rate constants (for the two interactions extracted from HL model, k_{on1}: black square, k_{on2}: red dot).

As the shape of the curves of the second interaction (figure S6 - insert) is characteristic of a non-specific interaction, we hypothesize that the second interaction is related to soluble RTX aggregates which can interact with the CD20 surface. This interpretation is reinforced by the variation of the normalized R_{max} with the CD20 density which is increasing for low CD20 densities (between 0 and 10 pmol.cm^{-2}). Self-association of RTX has been already mentioned in the literature and shown by using chromatography of exclusion.[4]

In conclusion, parameters related to the specific interaction are selected thanks to the magnitude and shape of the deconvolution curves.

7. SDS-PAGE analysis of Fab

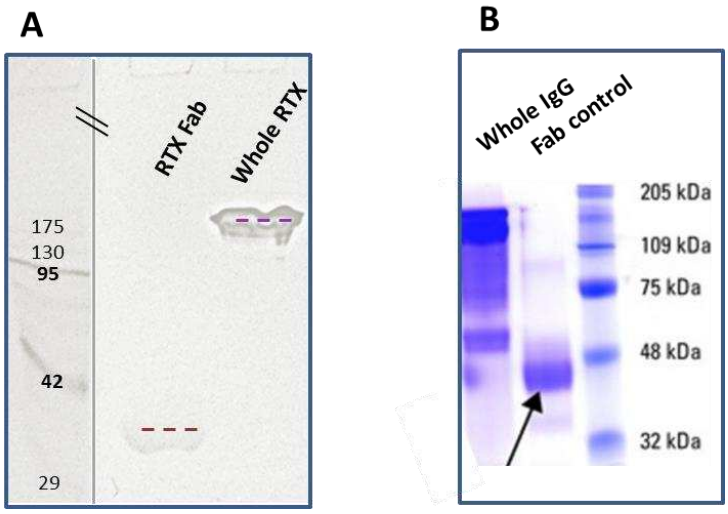

Figure S8. SDS-PAGE of IgG and its Fab fragment (A) experimental and (B) provided by Thermo Scientific.

8. Spectroscopic Ellipsometry (SE) experiments

Spectroscopic ellipsometry (SE) monitors the changes in ellipsometric angles ψ and Δ of polarized light upon reflection at a planar surface. SE is sensitive to changes in refractive index of the film and, by proper data treatment, provides access to the film refractive index and thickness, as well as the adsorbate surface density.

Experiments by QCM-D coupled with spectroscopic ellipsometry were performed in situ at a working temperature of 23 °C using a custom-designed open glass cuvette.[1] SAMs were formed on gold-coated QCM-D sensors using the same procedure as in QCM-D experiments. SE data were acquired with a spectroscopic rotating compensator ellipsometer (M2000V; J. A. Woollam, Lincoln, NE, USA) over a wavelength range of λ = 380-1000 nm, at 65° of angle of incidence. Before use, the inner surfaces of the glass cuvette were passivated by exposure to an aqueous solution of 10 $mg.mL^{-1}$ of bovine serum albumin for 10 min, rinsed with water and blow-dried with nitrogen gas. Before each experiment, measurements of the ellipsometric angles Δ and Ψ were performed on the SAM-coated surface in three distinct conditions: in air without any cuvette, in air with the sensor installed in the cuvette, and finally with the cuvette filled with ultrapure water. These steps are important to characterize SAM properties, and also to check for negligible window effects (as described in ref. 1). In situ measurements of the peptide grafting process consisted of obtaining a stable baseline in DMSO:H_2O (1:1) for a few minutes, injection of CD20 click solution at the desired final concentration, and rinsing in DMSO:H_2O (1:1) solution. During all steps, the cuvette content was continuously homogenised with the aid of a magnetic stirrer. For the rinsing step, the cuvette content was diluted by repeated addition of fresh DMSO:H_2O (1:1) solution and removal of excess liquid using a syringe needle connected to a peristaltic pump (Ismatec, Glattbrugg, Switzerland). The same procedure was performed to finally finish in water at pH 8.

The thickness and the refractive index of the layers (SAM and CD20) were determined through fitting of the data to optical models, using the software CompleteEASE (Woollam). The model relates the measured Δ and ψ as a function of λ to the optical properties of the sensor surface, the adsorbed film, and the surrounding solution. The semi-infinite bulk solution was treated as a transparent Cauchy medium, with a refractive index nsol(λ) = A_{sol} + B_{sol}/λ2. For pure water as bulk solution, A_{sol} = 1.322 and B_{sol} = 0.00322 μm^2 were used. Toward determination of the thickness of the CD20 layer, the opaque gold coating modified with SAM was treated as a homogeneous substrate. Its effective optical properties were determined from data acquired in the presence of bulk solution (pure water) but in the absence of a protein film, by fitting the refractive index and extinction coefficient over the accessible λ range using a B-spline algorithm implemented in CompleteEASE. The solvated CD20 layer was treated as a single layer, which we assumed to be transparent and homogeneous (Cauchy medium), with a given thickness d and refractive index n(λ) = A + B/λ2. Fitting was performed in pure water with d and A as fitting parameters, assuming B = Bsol. The χ2 value for the best fit was typically below 2, indicating a good fit. The best fit gave a CD20 layer thickness of 4.6 ± 0.2 nm and a refractive index of 1.42 ± 0.02 (for λ = 632.8 nm).

The thickness of the SAM was extracted using SE analysis in air. To this end, the surface was characterized before and after SAM formation. The optical properties of the gold coating were determined from data acquired prior to SAM formation, by fitting the refractive index and extinction coefficient over the accessible λ range using a B-spline algorithm. The SAM was treated as a Cauchy medium, and was found to be 2.5 ± 0.5 nm thick (with a refractive index of 1.29 ± 0.04, for λ = 632.8 nm).

9. QCM-D quantification of grafted peptide

Quartz crystal microbalance (QCM-D) monitors the changes in resonance frequency, Δf, and energy dissipation, ΔD, of the shear oscillation of a quartz crystal sensor upon binding and unbinding processes on the sensor surface. To a first approximation, Δf is related to the amount of bound material (including hydrodynamically coupled solvent) and ΔD is related to the softness of the interfacial film. In the case of homogeneous, quasi-rigid films the frequency shift is proportional to the mass uptake per unit area (mQCM), as described by the Sauerbrey:

$$m_{QCM} = -C\,\Delta f \qquad \text{(Eq. S2)}$$

Here, the mass sensitivity constant, C, is equal to 18.06 $ng.cm^{-2}.Hz^{-1}$ for sensors with a fundamental resonance frequency of f1 = 4.95 MHz. The areal mass density includes water hydrodynamically coupled to the organic film.

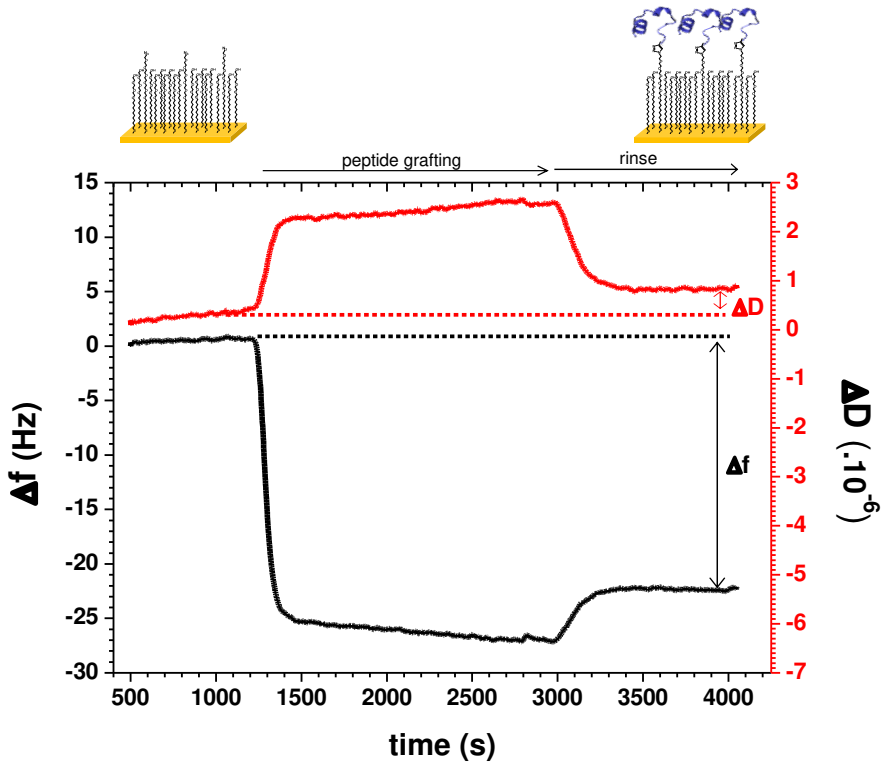

Figure S9. Example of a QCM-D profile recorded during the covalent grafting of CD20 epitope onto a SAM-azide functionalized surface prepared from a thiol mixture containing 12.5% of azide-terminated thiols. Black line: frequency shift; red line: dissipation shift. The duration of peptide grafting, and of the subsequent rinsing step, are indicated by arrows on top of the graph. A partial increase in frequency (and decrease in dissipation) is obtained when the surface is washed with the rinsing solution due to differences in the density and/or viscosity of the rinsing solution compared to the peptide grafting solution, and possibly also due to release of non-specifically bound reagents. The QCM-D signals after rinsing confirm the stability of the surface.

As expected, for a surface without azide function no measurable shift in frequency was detected when comparing before and after incubation with the CD20 antigen, signifying that there is no stable yet unspecific peptide adsorption on the surface (Fig. S7). Changes in frequency during incubation with the peptide solution are likely due to solution effects. The higher rate of change in frequency recorded during the rinsing step (compared to that of the injection step) is due to a variation of the flow rate, 5 µL/min for the injection and 20 µL/min for the rinsing.

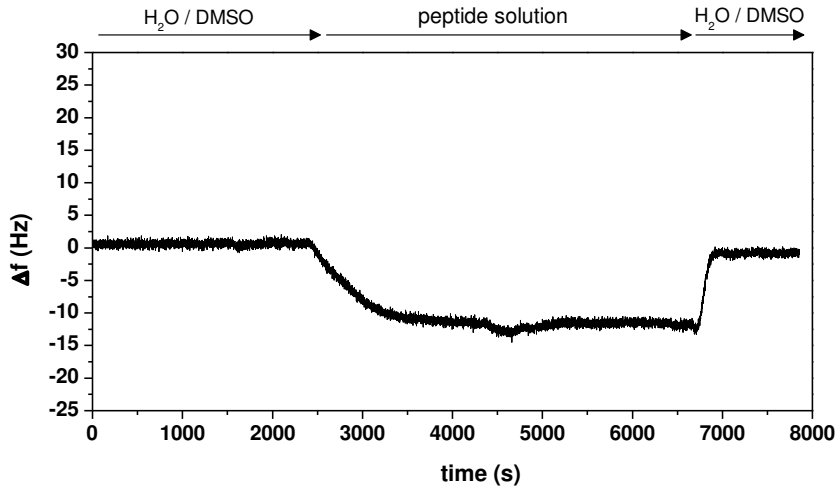

Figure S10. QCM-D profile (change in resonance frequency) characterizing the absence of CD20 grafting onto a surface without azide.

10. Calculation of the CD20 hydration layer

The hydration H of the CD20 layer is deduced from equation S3:

$$H = (m_{QCM} - m_{SPR}) \times 100/m_{QCM} \qquad \text{(Eq. S3)}$$

with mSPR the optical mass (determined by Jung's formula; Eq. S1) and m_{QCM} the acoustic mass (determined with Sauerbrey's equation; Eq. S2).

11. Specificity of CD20 functionalized surface towards RTX binding – QCM-D experiment

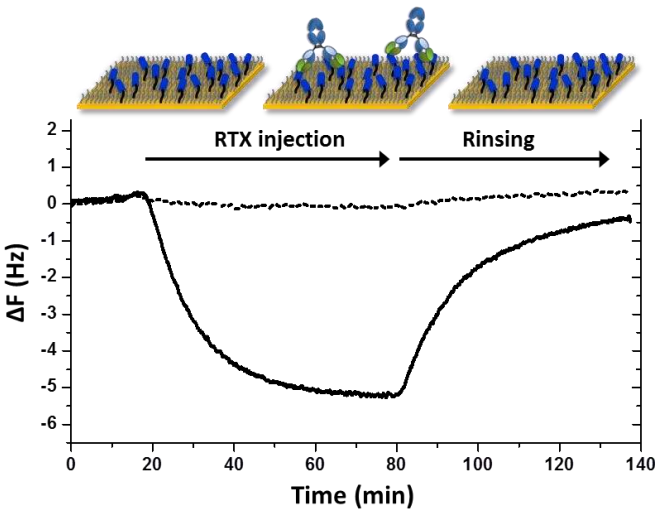

Figure S11. QCM-D profiles characterizing CD20 – RTX recognition. 10 nM RTX in phosphate buffered saline (PBS) with 3 mM citrate and 0.005% P80 was injected on 20% azide-functionalized surfaces that display CD20 (solid line) and CD20 scramble (dashed line). T = 25°C, flow rate = 10 µL.min^{-1}.

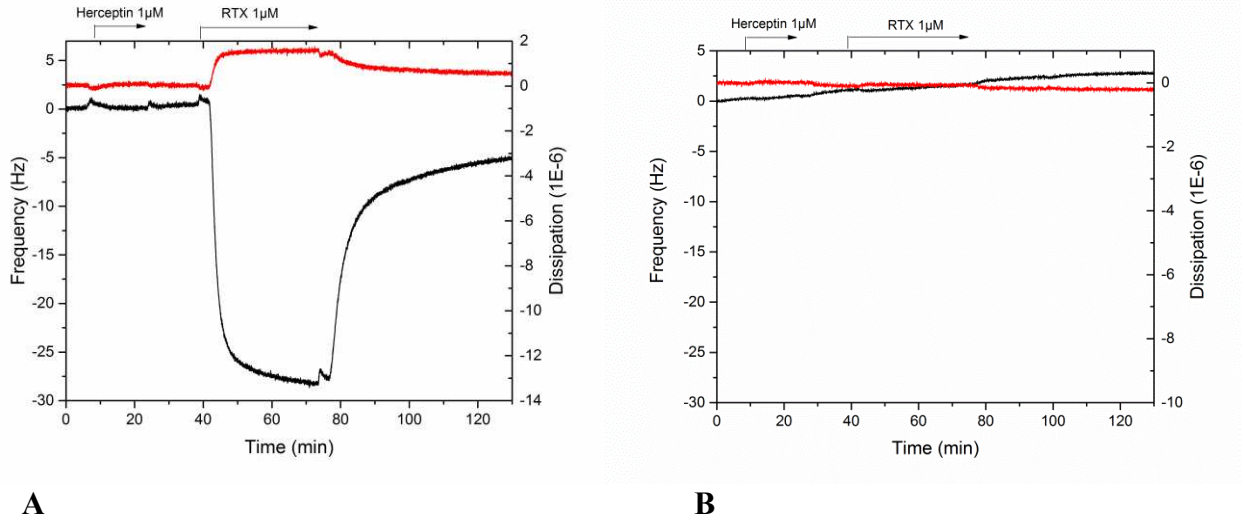

Figure S12. QCM-D profiles characterizing the specific recognition of RTX. (A) CD20 functionalized surface and (B) N_3-terminated SAM surface prepared from a thiol solution containing 10% of N_3-terminated thiol, first injection of 1µM Herceptin and second injection of 1µM RTX in phosphate buffered saline (PBS), 3 mM citrate, 0.005% P80. T = 25°C, flow rate = 10 µL.min^{-1}.

12. Calculation of the available CD20 antigens on SAM substrate

Considering the organization of the surface, it is unlikely that all CD20 antigens grafted to the surface can be fully implicated in RTX binding. Yang et al [5] have developed a model (adapted from a previous model reported by Hlavacek et al [6] characterizing the surface association in bivalent systems) with the objective of calculating the available ligand density for subsequent mAb binding to an antigen functionalized surface. According to this model some ligands may be available, whereas others are already bound in another interaction, or unavailable because they are covered by an analyte, or because a neighboring ligand obstructs binding. The probability of a ligand being available for binding can be expressed as the product of: (1) the probability that a ligand is not bound to a surface adsorbed mAb, (2) the probability that an unbound ligand is not covered by the mAb and (3) the probability that an unbound and uncovered ligand is not excluded from binding by its close proximity to a surface bound mAb.[6]

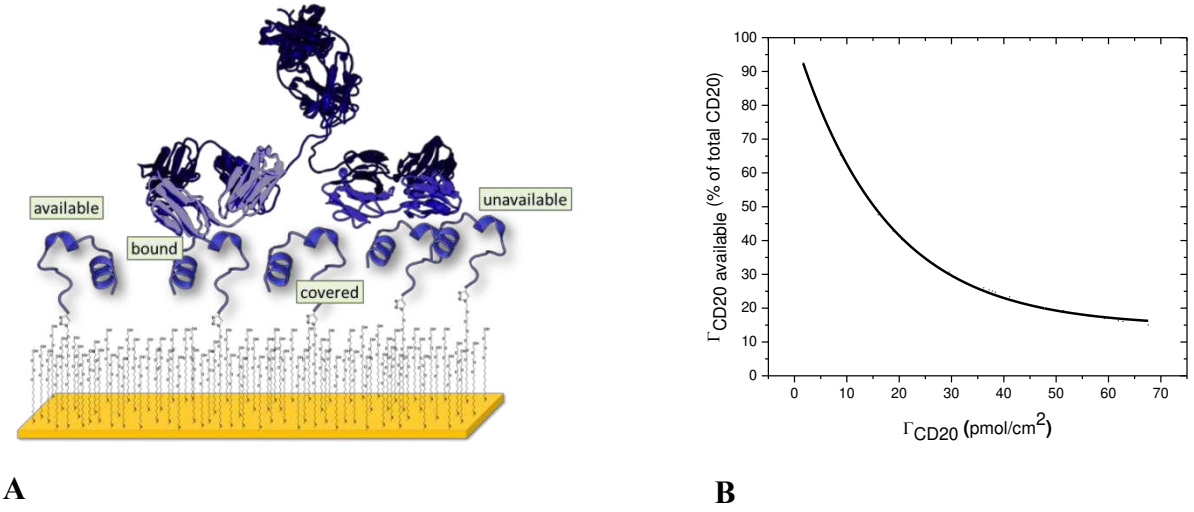

Figure S13. (A) Possible states that can be adopted by CD20 antigens on a surface; (B) Visualization of the percentage of available antigens.

The calculation of available CD20 is based on this model, where the authors calculated the probability of a ligand being available for binding when i sites are already bound. The fraction of bound sites is i/n, where n is the total number of sites. The number of i sites are calculated with equation S4.

$$i = \frac{(2 + \frac{0.5na}{A}) \pm \sqrt{4 + \left(\frac{0.5na}{A}\right)^2}}{a/A} \qquad \text{(Eq. S4)}$$

where a is the area covered by an IgG antibody (60 nm^2), and n/A the density of grafted CD20 antigen calculated from SPR experiments.

The available ligand density for binding is:

$$\Gamma_{CD20}\, available = 2(n-i) + \frac{i\,a(-n+i)}{A} \qquad \text{(Eq. S5)}$$

The results show that almost all CD20 are available (81%) for 1% of azide (Γ_{CD20} = 2.8 $pmol.cm^{-2}$), but only 21% are available for 12.5% (Γ_{CD20} = 46 $pmol.cm^{-2}$).

13. Determination of the binding affinity using QCM-D

The variation of KD as a function of CD20 surface densities has also been evaluated by QCM-D. To this end, RTX-CD20 binding assays were performed by QCM-D for three different azide-functionalized SAMs: 2.5, 12.5, and 50%. RTX concentrations used are:

For 2.5% thiol-azide: 10, 25, 50, 100, 250, 500, 1000, 2000 nM

For 12.5% thiol-azide: 5, 10, 50, 100, 250, 500, 1000, 2000 nM

For 50% thiol-azide: 0.05, 0.1, 0.5, 1, 2, 4, 6, 9 µM

For each RTX concentration the frequency shifts at equilibrium were plotted as a function of RTX concentration and the resulting Langmuir isotherms were fitted with equation S7 in order to obtain the apparent $K_{D,app}$.

$$\Delta f_{CD20-RTX} = \Delta f_{\max} \frac{[RTX]}{K_{Dapp} + [RTX]} \quad \text{(Eq. S6)}$$

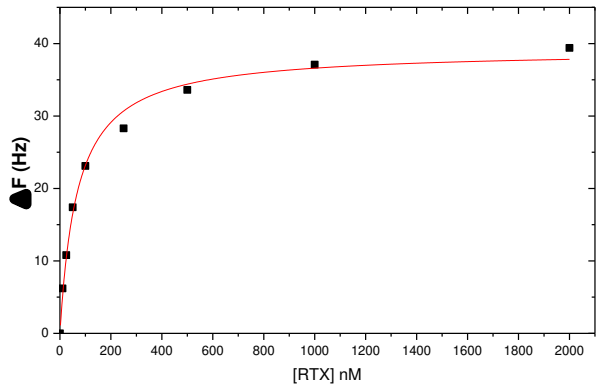

Figure S14. Example of the Langmuir isotherm obtained for the 2.5% functionalized surface.

Table S2. Comparison of CD20-RTX KD obtained from QCM-D or SPR.

% N_3	$K_{D\ \text{QCM-D}}$ (nM)	$K_{D\ \text{SPR}}$ (nM)
2.5	68.7 ± 6.8	75 ± 6
12.5	17.9 ± 3.4	32 ± 12
50	13049 ± 1372.9	1007 ± 16

As we can see in Table S2, values found in QCM-D and SPR are in the same order of magnitude in the case of surfaces with 2.5 and 12.5% of azide functions. However, the gap is more pronounced at 50%, where the K_D calculated in QCM-D is much higher (out of the concentrations injected). The trend is though still the same; and in both cases, affinity ranking is identical: K_D (12.5%) > K_D (2.5%) > K_D (50%).

14. Fab binding assays

Fab binding assays were performed in the same conditions as for RTX. Fig. S15 illustrates two sets of sensorgrams obtained for CD20 surface densities discussed in the manuscript (2.0 and 46 pmol.cm^{-2}).

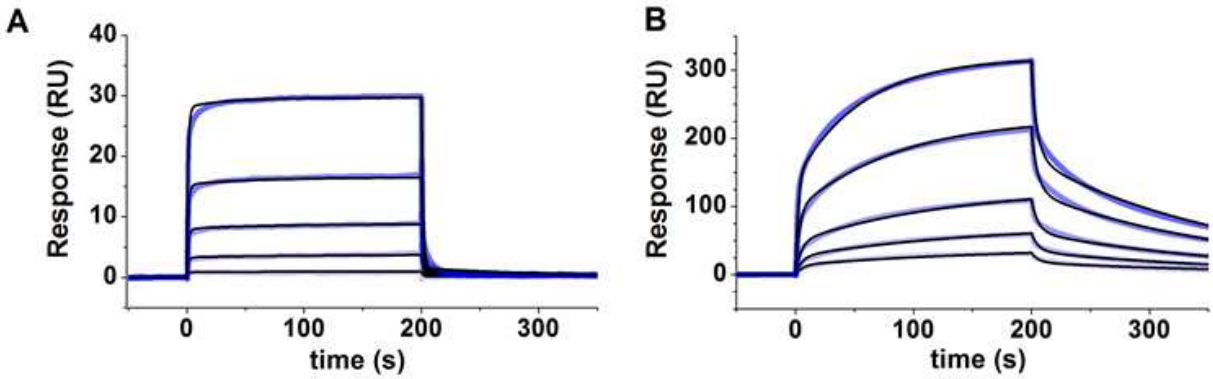

Figure S15. RTX Fab - CD20 SPR binding profiles. Sensorgrams were recorded at different CD20 surface densities: (A) 2.8 pmol.cm^{-2}, and (B) 46 pmol.cm^{-2}. The Fab fragment concentrations were 50, 200, 500, 1000 nM for 2.8 pmol.cm^{-2}, and from 50, 100, 200, 500, 1000 nM for 46 pmol.cm^{-2}. The sensorgrams were fitted with the heterogeneous ligand kinetic model (RI correction = 0) and the fitted curves were added to the graph (black curves).

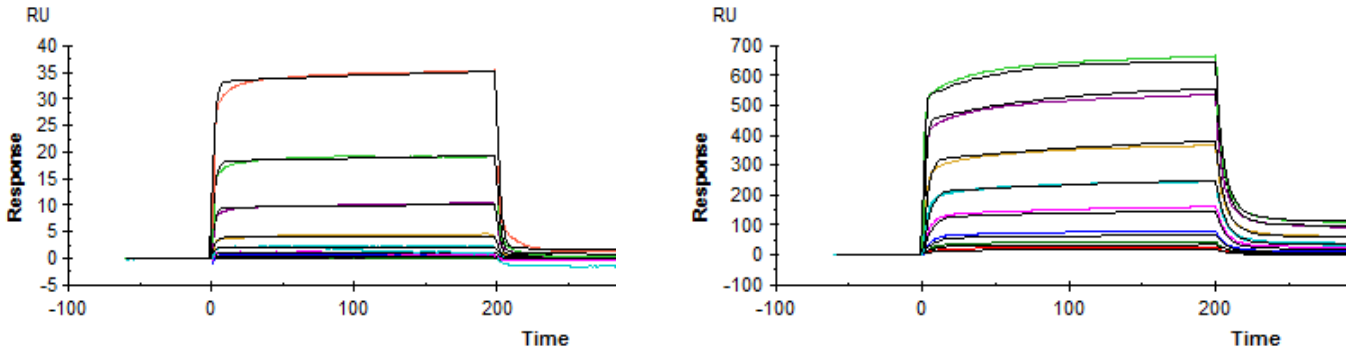

(A) RTX Fab-CD20 SPR binding profiles (colored curves), black curves are the fitted curves (heterogeneous ligand kinetic model: k_a= 0.5 10^5 $M^{-1}.s^{-1}$)

(B) RTX-CD20 SPR binding profiles (colored curves), black curves are the fitted curves (heterogeneous ligand kinetic model: ka=18.5 10^5 $M^{-1}s^{-1}$)

Figure S16. Examples of sensorgrams recorded on the same CD20 functionalized sensor chip bearing 2.8 pmol.cm^{-2} (prepared from thiol solution containing 1% of azide) for Fab fragment (A) and for RTX (B) concentrations of 5, 10, 20, 50, 100, 200, 500, 1000 nM.

15. References

1. Jung, L. S.; Campbell, C. T.; Chinowsky, T. M.; Mar, M. N.; Yee, S. S. *Langmuir* **1998**, *14*, 5636–5648.
2. a) Dejeu, J.; Bonnet, H.; Spinelli, N.; Defrancq, E.; Coche-Guerente, L.; Van der Heyden, A.; Labbé, P. *J. Phys. Chem. C* **2018**, *122*, 21521-21530 ; b) Mac Donald, H.; Bonnet, H.; Van der Heyden, A.; Defrancq, E.; Spinelli, N.; Coche-Guérente, L.; Dejeu, J. *J. Phys. Chem. C* **2019**, *123*, 13561-13568.
3. Schoch, R. L.; Kapinos, L. E.; Lim, R. Y. H. *Proc. Natl. Acad. Sci.* **2012**, *109*, 16911–16916.
4. Morgan, H.; Tseng, S.-Y.; Gallais, Y.; Leineweber, M.; Buchmann, P.; Riccardi, S.; Nabhan, M.; Lo, J.; Gani, Z; Szely, N.; Zhu, C. S.; Yang, M.; Kiessling, A.; Vohr, H.-W.; Pallardy, M.; Aswad, F.; Turbica, I. *Front. Immunol.* **2019**, *10*:601. doi: 10.3389/fimmu.2019.00601.
5. Yang, T.; Baryshnikova, O. K.; Mao, H.; Holden, M. A.; Cremer, P. S. *J. Am. Chem. Soc.* **2003**, *125*, 4779–4784.
6. Hlavacek, W. S.; Posner, R. G.; Perelson, A. S. *Biophys. J.* **1999**, *76*, 3031–3043.